Composition and thermodynamics of nuclear matter with light clusters

S. Typel,[1,2,*] G. Röpke,[3,†] T. Klähn,[4,5,‡] D. Blaschke,[5,6,§] and H. H. Wolter[7,‖]

[1]*Excellence Cluster Universe, Technische Universität München, Boltzmannstraße 2, D-85748 Garching, Germany*

[2]*GSI Helmholtzzentrum für Schwerionenforschung GmbH, Theorie, Planckstraße 1, D-64291 Darmstadt, Germany*

[3]*Institut für Physik, Universität Rostock, Universitätsplatz 3, D-18051 Rostock, Germany*

[4]*Theory Group, Physics Division, Building 203, Argonne National Laboratory, 9700 South Cass Avenue, Argonne, Illinois 60439, USA*

[5]*Instytut Fizyki Teoretycznej, Uniwersytet Wrocławski, Max Born Place 9, 50-204 Wrocław, Poland*

[6]*Bogoliubov Laboratory for Theoretical Physics, JINR Dubna, Joliot-Curie Street 6, 141980 Dubna, Russia*

[7]*Fakultät für Physik, Universität München, Am Coulombwall 1, D-85748 Garching, Germany*

(Received 20 August 2009; published 13 January 2010)

We investigate nuclear matter at a finite temperature and density, including the formation of light clusters up to the α particle ($1 \leqslant A \leqslant 4$). The novel feature of this work is to include the formation of clusters as well as their dissolution due to medium effects in a systematic way using two many-body theories: a microscopic quantum statistical (QS) approach and a generalized relativistic mean-field (RMF) model. Nucleons and clusters are modified by medium effects. While the nucleon quasiparticle properties are determined within the RMF model from the scalar and vector self-energies, the cluster binding energies are reduced because of Pauli blocking shifts calculated in the QS approach. Both approaches reproduce the limiting cases of nuclear statistical equilibrium (NSE) at low densities and cluster-free nuclear matter at high densities. The treatment of the cluster dissociation is based on the Mott effect due to Pauli blocking, implemented in slightly different ways in the QS and the generalized RMF approaches. This leads to somewhat different results in the intermediate density range of about 10^{-3} to 10^{-1} fm^{-3}, which gives an estimate of the present accuracy of the theoretical predictions. We compare the numerical results of these models for cluster abundances and thermodynamics in the region of medium excitation energies with temperatures $T \leqslant 20$ MeV and baryon number densities from zero to a few times saturation density. The effects of cluster formation on the liquid-gas phase transition and on the density dependence of the symmetry energy are studied. It is demonstrated that the parabolic approximation for the asymmetry dependence of the nuclear equation of state breaks down at low temperatures and at subsaturation densities because of cluster formation. Comparison is made with other theoretical approaches, in particular, those that are commonly used in astrophysical calculations. The results are relevant for heavy-ion collisions and astrophysical applications.

DOI: 10.1103/PhysRevC.81.015803 PACS number(s): 21.65.Mn, 26.50.+x, 21.30.Fe, 25.75.−q

I. INTRODUCTION

The composition and the equation of state (EoS) of nuclear matter, possible phase transitions, or condensates are widely discussed in several areas of nuclear physics. They attain an increasing importance in astrophysics and cosmology. Many of the systems under consideration have large charge asymmetries and cover a broad range of densities. Therefore, a deeper understanding of the composition and the thermodynamical properties of nuclear matter and, in particular, the density dependence of the symmetry energy, from very low saturation densities to supersaturation densities, is of great interest. Let us mention three examples of systems where the knowledge of the symmetry energy in a broad range of densities is of crucial importance: (1) the surface structure of exotic nuclei with large neutron excess or new exotic collective modes, (2) the structure and composition of neutron stars from the ultradense core to the crust at subsaturation densities with varying asymmetry due to β equilibrium, and (3) core collapse supernovae, where at high densities the symmetry energy determines the energy of the shock and at low densities it affects the nuclear composition, neutrino interactions, and aspects of nucleosynthesis.

This wide spectrum of applications illustrates the importance of gathering reliable information on the EoS of nuclear matter and, specifically, the symmetry energy, since predictions of its density dependence differ strongly for different theoretical approaches. Therefore, considerable effort has been made to obtain constraints from observational data on all aspects of the EoS. A promising source of information arises from the study of heavy-ion collisions, where transient states of very different densities can be investigated and the asymmetry can be varied to a certain extent by choosing the collision system. Central collisions at high energies yield large compressions and provide information from observations of nucleon flow [1] and particle production as shown for kaons, for example, in Refs. [2,3]. Recent reviews of studies of the symmetry energy in heavy-ion collisions were given in Refs. [4–6].

Recently, particular interest has been devoted to the properties of nuclear and neutron matter at very low densities, down to the limit of zero density. Below saturation density, correlations are expected to become important and nuclear matter can become inhomogeneous. An aspect of this is seen in

*s.typel@gsi.de
†gerd.roepke@uni-rostock.de
‡thomas.klaehn@googlemail.com
§blaschke@ift.uni.wroc.pl
‖hermann.wolter@physik.uni-muenchen.de

fragmentation as a signature of the liquid-gas phase transition. At even smaller densities, down to one hundredth or one thousandth of saturation density and at moderate temperatures, few-body correlations remain important. This results from the fact that at low densities the system can minimize its energy by forming light clusters such as deuterons, or particularly strongly bound α particles. With increasing density such clusters will dissolve as a result of the Pauli principle. Thus there exists an interesting detailed evolution of the correlations and the composition in nuclear matter depending on the density and temperature that presents a challenge to a theoretical description.

In the laboratory, low-density matter occurs in the outer regions of heavy nuclei, in halo nuclei, in expanding hot matter from heavy-ion reactions, in the envelopes of core-collapse supernovae, and also in recently discussed low-density isomeres such as the Hoyle state of ^{12}C [7]. Experimental information on the composition and behavior of very-low-density nuclear matter was recently obtained by Kowalski *et al.* [8] from the observation of the light particles emitted in low-energy heavy-ion collisions. It was found that the fraction of light particles is substantial at very low densities, implying a finite symmetry energy in the limit of zero density.

Nonrelativistic Skyrme Hartree-Fock and relativistic mean-field calculations revealed a tight correlation between the density derivative of the neutron matter EoS near 2/3 of the saturation density and the neutron skin thickness ΔR_{np} of heavy nuclei [9,10]. This observation translates into a correlation of the density dependence of the symmetry energy at saturation density with ΔR_{np} [6,11–16]. The scheduled PREX experiment at JLab is expected to provide a precise value of the neutron skin thickness of ^{208}Pb from the observation of parity violations in electron scattering [17], hence providing an independent constraint on the density dependence of the symmetry energy.

At densities beyond nuclear saturation constraints on the EoS are expected in increasing quality from neutron star observables such as masses, mass-radius relations, gravitational binding energy, and the cooling behavior of neutron stars. A recent review by Klähn *et al.* [18] discusses these constraints in confrontation with those from heavy-ion collisions. It demonstates that at present it is far from trivial to obtain an EoS that is consistent with all these available observational data. The study of exotic structures like pasta phases in the inner crust of neutron stars gives information on very-neutron-rich matter around normal densities [19–23].

The actual composition of very-low-density matter is also relevant for the investigation of various stages in supernova explosions as pointed out in a number of recent publications. It is known to affect the effectiveness of the neutrino reheating of the shock wave [24]. Also, the stellar core collapse is mostly determined during the dynamical plunge phase at densities between 10^{12} and 10^{14}g/cm^3, where temperatures between 10^{10} K and 10^{11} K are reached [25,26]. The sensitivity of the collapse dynamics on the properties of matter in this density regime could strongly influence the structure and composition of the protoneutron star [27] and possible gravitational wave and neutrino signals emitted at various stages during and after core bounce.

Only very few models for the EoS are applicable in actual supernova simulations. The reason is found in the required wide range of temperatures, densities, and asymmetries, which either are not available, for example, in tabular form, or are not covered by the model. The most frequently used EoS are those of Lattimer and Swesty [28] and of Shen *et al.* [29]. The former one is based on an extended liquid drop model for the nuclei embedded in a nucleon and α-particle gas, whereas the latter one has been developed in the framework of the relativistic mean-field (RMF) approach with nonlinear meson self-couplings [30]. Shen *et al.* [29] use the Thomas-Fermi approximation to describe heavy nuclei embedded in a gas. They consider α particles as a separate species, using an excluded volume prescription to model the dissolution of α particles at high densities, which accounts for medium effects only in a very global way. The model neglects other light clusters such as deuterons, tritons, and helions (^{3}He).

The problem of cluster formation in low-density nuclear matter has been addressed recently based on a virial expansion [31] to obtain the EoS for nuclear matter at all asymmetries including nucleons and α particles (^{4}He) [32] and in later work also tritons and helions [33] (see also Ref. [34] for a closely related formulation in an S-matrix approach and the quasiparticle gas model [35]). The virial coefficients in the Beth-Uhlenbeck approach [36] are given by the cluster-bound state energies and scattering phase shifts. In Ref. [32] these were taken directly from experiment, thus providing an exact limit for the EoS at very low densities, where the scattering is not yet influenced by medium effects. These results are believed to be reliable for densities up to $n_{\rm sat}/1000$ and not too small temperatures. They provide a benchmark for other calculations.

The present article emphasizes that correlations, in-medium modifications of cluster properties, and mean-field effects must be considered simultaneously in the description of low-density nuclear matter, because all these affect the thermodynamical properties of the EoS. The occurrence of clusters also changes the symmetry energy because the cluster correlations depend on the asymmetry of the system. Here we restrict ourselves to matter in thermodynamic equilibrium at temperatures $T \leqslant 20\,\mathrm{MeV}$ and baryon number densities $n \leqslant 0.2\,\mathrm{fm}^{-3}$, where the quark substructure and excitations of internal degrees of freedom of nucleons (protons and neutrons) are not important and the nucleon-nucleon interaction can be represented by an effective interaction potential.

In this work, we explore two approaches to the problem: One is a quantum statistical (QS) formulation based on the thermodynamic Green function method [37]. This approach makes explicit use of an effective nucleon-nucleon interaction. It allows us to account for medium effects on the cluster properties. The second approach is a generalized RMF model, where the medium-modified clusters are introduced as explicit degrees of freedom. The two methods have their strengths and deficiencies. The RMF method is reliable to determine the nucleon quasiparticle propagator in the medium, and this information is introduced into the QS model. The QS model, however, can determine the medium modifications of the clusters, such as the mass shift and the (momentum-dependent)

Mott densities, where the clusters get dissolved. These are then introduced in parametrized form into the RMF method.

The particle number density $n_\tau(T, \mu_p, \mu_n)$ of protons ($\tau = p$) or neutrons ($\tau = n$) depends on the temperature T and the chemical potentials μ_τ. In the QS approach it is obtained from the single-particle spectral function, which can be expressed in terms of the self-energy. This is the main quantity to be evaluated. Considering the ladder approximation [37,38], the formation of bound states is taken into account in a Bethe-Goldstone equation that in the low-density limit reduces to an effective Schrödinger equation. Effects of the medium can be included in a self-consistent way within the cluster mean-field approximation (for references, see [38–40]). The bound-state energies are also modified because of Pauli blocking in the correlated medium. An extended discussion of the two-particle problem can be found in Ref. [41]. This generalized Beth-Uhlenbeck formulation accounts for medium effects suppressing correlations at high densities. It allows one to determine the second virial coefficient and also contains the Brueckner approach to matter near saturation density. The approach has been extended to three- and four-particle bound states in Refs. [38,42]. The medium-dependent shift of the cluster binding energies has been investigated in Refs. [43,44]. We emphasize again that this quantum statistical approach avoids the introduction of semi-empirical concepts such as the excluded volume mechanism to mimic in-medium effects. However, because the quasiparticle propagator is introduced from the outside (i.e., from the RMF model), the back effect of the clusters on the mean field is not included.

The RMF model, in contrast, takes this back reaction fully into account. However, only the bound-state contributions of the clusters are included (from the QS model). Thus the continuum contributions are missing, which, as we shall see, leads to an overestimation of the two-particle correlations. Thus, by investigating both these models we also obtain an estimate of the remaining uncertainties of theoretical approaches. Also, in the present work, in both approaches, we have not yet included the contribution of heavier clusters, which should appear in the intermediate density range before the matter becomes homogenous again at densities near saturation. This problem will be addressed in a later work.

Extending the quasiparticle approach including the formation of light clusters enables us to describe the smooth transition from the low-density limit, where the nuclear statistical equilibrium (NSE) or the virial expansion are applicable, to the region of the saturation density where mean-field concepts have been successfully applied. None of the existing approaches to model the EoS gives satisfactory results in both regions simultaneously. More precisely, the EoS of Lattimer and Swesty [28] as well as the EoS of Shen *et al.* [29] fail to reproduce the NSE in the low-density limit, whereas the EoS in the virial expansion [31–33] ignores medium effects on light clusters and cannot describe the dissolution of clusters at high densities.

The outline of this article is as follows: In Sec. II we review the QS approach to the EoS and put particular emphasis on the calculation of the medium modifications of the clusters. As one result we obtain a density- and temperature-dependent modification of the binding energies of the clusters. In Sec. III we introduce our generalized RMF model with light clusters as explicit degrees of freedom. We use a RMF model with density-dependent meson-nucleon couplings [45], which has been used very successfully to describe nuclear structure in a wide region of the nuclear chart and has also been tested in heavy-ion collisions. The medium-dependent masses of the clusters lead to a coupling of the nucleon and cluster dynamics. We also show how the thermodynamic quantities, such as free and internal energy, pressure, and entropy are obtained as functions of density and temperature. In Sec. IV we discuss the composition of nuclear matter and present the thermodynamical quantities for symmetric nuclear matter in both approaches. We also compare to the NSE model that gives the correct low-density limit. Of particular interest is the phase transition from the (partially) clusterized to the homogeneous medium, which is considered in Sec. V. In Sec. VI we discuss specifically the symmetry energy of nuclear matter as a function of density and temperature, which is drastically changed at very low densities because of the cluster correlations. In Sec. VII we finally compare the results for the α cluster fraction in the QS and generalized RMF models with previous approaches and discuss the advantages of the present ones. We close with an outlook on further work, which should finally lead to an EoS that can be used in a wide range of problems, including nuclear structure, heavy-ion reactions, and supernovae simulations. Throughout the article we use natural units where $\hbar = c = k_B = 1$.

II. QUANTUM STATISTICAL APPROACH TO THE EQUATION OF STATE

A. Single-particle spectral function and quasiparticles

Using the finite-temperature Green function formalism, a nonrelativistic quantum statistical approach can be given to describe the equation of state of nuclear matter including the formation of bound states [38,41]. It is most convenient to start with the nucleon number densities $n_\tau(T, \tilde{\mu}_p, \tilde{\mu}_n)$ as functions of temperature T and nonrelativistic chemical potentials $\tilde{\mu}_\tau$ for protons ($\tau = p$) and neutrons ($\tau = n$), respectively,

$$n_\tau(T, \tilde{\mu}_p, \tilde{\mu}_n) = \frac{1}{\Omega}\sum_1 \langle a_1^\dagger a_1\rangle \delta_{\tau,\tau_1} = 2\int \frac{d^3k_1}{(2\pi)^3}\int_{-\infty}^{\infty}\frac{d\omega}{2\pi} f_{1,Z}(\omega) S_1(1,\omega), \quad (1)$$

where Ω is the system volume, $\{1\} = \{k_1, \sigma_1, \tau_1\}$ denotes the single-nucleon quantum numbers momentum, spin, and isospin. Summation over spin yields the factor 2 and

$$f_{A,Z}(\omega) = (\exp\{\beta[\omega - Z\tilde{\mu}_p - (A - Z)\tilde{\mu}_n]\} - (-1)^A)^{-1} \quad (2)$$

is the Fermi or Bose distribution function, which depends on the inverse temperature $\beta = 1/T$. The nonrelativistic chemical potential $\tilde{\mu}_\tau$ is related to the relativistic chemical potential μ_τ by $\mu_\tau = \tilde{\mu}_\tau + m_\tau$ with the nucleon mass m_τ. Instead of the isospin quantum number τ we occasionally use the mass number A and the charge number Z. Both the distribution function and the spectral function $S_1(1, \omega)$ depend on the

temperature and the chemical potentials $\tilde{\mu}_p$ and $\tilde{\mu}_n$, not given explicitly. We work with a grand canonical ensemble and have to invert Eq. (1) to write the chemical potentials as functions of the densities n_p and n_n. For this EoS, expressions such as the Beth-Uhlenbeck formula and its generalizations have been derived [32,38,41].

We consider both the total number densities of protons and neutrons, $n_p^{\rm tot}$ and $n_n^{\rm tot}$, and the temperature T as given parameters. Alternatively, the total baryon density $n = n_n^{\rm tot} + n_p^{\rm tot}$ and the asymmetry of nuclear matter $\delta = (n_n^{\rm tot} - n_p^{\rm tot})/n = 1 - 2Y_p$ are used. Y_p denotes the total proton fraction. In addition to the frozen equilibrium where $n_p^{\rm tot}$ and $n_n^{\rm tot}$ are given, we assume homogeneity and isotropy in space. Thermodynamical stability is considered in Secs. V and IV B. In a further development, allowing for weak interactions, β equilibrium may be considered, which is of interest for astrophysical applications. In that case the asymmetry δ is uniquely determined for given n and T.

The spectral function $S_1(1,\omega)$ is related to the self-energy $\Sigma(1,z)$ according to

$$S_1(1,\omega) = \frac{2\,\mathrm{Im}\,\Sigma(1,\omega - i0)}{[\omega - E(1) - \mathrm{Re}\,\Sigma(1,\omega)]^2 + [\mathrm{Im}\,\Sigma(1,\omega - i0)]^2}, \tag{3}$$

where the imaginary part has to be taken for a small negative imaginary part in the frequency ω. $E(1) = k_1^2/(2m_1)$ is the kinetic energy of the free nucleon. The solution of the relation

$$E_1^{\rm qu}(1) = E(1) + \mathrm{Re}\,\Sigma\big[1, E_1^{\rm qu}(1)\big] \tag{4}$$

defines the single-nucleon quasiparticle energies $E_1^{\rm qu}(1) = E(1) + \Delta E^{\rm SE}(1)$. Expanding for small $\mathrm{Im}\,\Sigma(1,z)$, the spectral function yields a δ-like contribution. The densities are calculated from Fermi distributions with the quasiparticle energies so that

$$n_\tau^{\rm qu}(T,\tilde{\mu}_p,\tilde{\mu}_n) = \frac{2}{\Omega}\sum_{k_1} f_{1,Z}\big[E_1^{\rm qu}(1)\big] \tag{5}$$

follows for the EoS in mean-field approximation. This result does not contain the contribution of bound states and therefore fails to be correct in the low-temperature, low-density limit where the NSE describes the nuclear matter EoS.

As shown in Refs. [38,41], the bound-state contributions are obtained from the poles of $\mathrm{Im}\,\Sigma(1,z)$, which cannot be neglected in expanding the spectral function with respect to $\mathrm{Im}\,\Sigma(1,z)$. A cluster decomposition of the self-energy has been proposed, see Ref. [38]. The self-energy is expressed in terms of the A-particle Green functions, which read in bilinear expansion

$$G_A(1\ldots A, 1'\ldots A', z_A) = \sum_{\nu K} \psi_{A\nu K}(1\ldots A)\frac{1}{z_A - E_{A,\nu}^{\rm qu}(K)} \times \psi^*_{A\nu K}(1'\ldots A'). \tag{6}$$

The A-particle wave function $\psi_{A\nu K}(1\ldots A)$ and the corresponding eigenvalues $E_{A,\nu}^{\rm qu}(K)$ result from solving the in-medium Schrödinger equation (see the following subsections). K denotes the center-of-mass momentum of the A-nucleon system. In addition to the bound states, the summation over the internal quantum states ν includes also the scattering states.

The evaluation of the equation of state in the low-density limit is straightforward. Considering only the bound-state contributions, we obtain the result

$$\begin{aligned} n_p^{\rm tot}(T,\tilde{\mu}_p,\tilde{\mu}_n) &= \frac{1}{\Omega}\sum_{A,\nu,K} Z f_{A,Z}\big[E_{A,\nu}^{\rm qu}(K;T,\tilde{\mu}_p,\tilde{\mu}_n)\big], \\ n_n^{\rm tot}(T,\tilde{\mu}_p,\tilde{\mu}_n) &= \frac{1}{\Omega}\sum_{A,\nu,K} (A-Z) f_{A,Z}\big[E_{A,\nu}^{\rm qu}(K;T,\tilde{\mu}_p,\tilde{\mu}_n)\big], \end{aligned} \tag{7}$$

for the EoS describing a mixture of components (cluster quasiparticles) obeying Fermi or Bose statistics. The total baryon density results as $n(T,\tilde{\mu}_p,\tilde{\mu}_n) = n_n^{\rm tot}(T,\tilde{\mu}_p,\tilde{\mu}_n) + n_p^{\rm tot}(T,\tilde{\mu}_p,\tilde{\mu}_n)$. To derive the extended Beth-Uhlenbeck formula, see Ref. [42], we restrict the summation to $A \leqslant 2$, but extend the summation over the internal quantum numbers ν, not only to the excited states but also to the scattering states. Note that at low temperatures Bose-Einstein condensation may occur.

The NSE is obtained in the low-density limit if the in-medium energies $E_{A,\nu}^{\rm qu}(K;T,\tilde{\mu}_p,\tilde{\mu}_n)$ can be replaced by the binding energies of the isolated nuclei $E_{A,\nu}^{(0)}(K) = E_{A,\nu}^{(0)} + K^2/(2Am)$, with $m = 939\,\mathrm{MeV}$ the average nucleon mass. For the cluster contributions, that is, $A > 1$, the summation over the internal quantum numbers is again restricted to the bound states only. We have

$$\begin{aligned} n_p^{\rm NSE}(T,\tilde{\mu}_p,\tilde{\mu}_n) &= \frac{1}{\Omega}\sum_{A,\nu,K}^{\rm bound} Z f_{A,Z}\big[E_{A,\nu}^{(0)}(K)\big], \\ n_n^{\rm NSE}(T,\tilde{\mu}_p,\tilde{\mu}_n) &= \frac{1}{\Omega}\sum_{A,\nu,K}^{\rm bound} (A-Z) f_{A,Z}\big[E_{A,\nu}^{(0)}(K)\big]. \end{aligned} \tag{8}$$

The summation over A includes also the contribution of free nucleons, $A = 1$.

In the nondegenerate and nonrelativistic case, assuming a Maxwell-Boltzmann distribution, the summation over the momenta K can be performed analytically and the thermal wavelength $\lambda = \sqrt{2\pi/(mT)}$ of the nucleon enters. As shown below, the medium effects in nuclear matter are negligible below 10^{-4} times the saturation density $n_{\rm sat}$ for the temperatures considered here.

Interesting quantities are the mass fractions

$$X_{A,Z} = \frac{A}{\Omega n}\sum_{\nu,K} f_{A,Z}\big[E_{A,\nu}^{\rm qu}(K;T,\tilde{\mu}_p,\tilde{\mu}_n)\big] \tag{9}$$

of the different clusters. From the EoS considered here, thermodynamical potentials can be obtained by integration, in particular the free energy per volume F/Ω. In the special case of symmetric nuclear matter, $Y_p^{\rm s} = 0.5$, the free energy per volume is obtained from the averaged chemical potential $\tilde{\mu} = (\tilde{\mu}_p + \tilde{\mu}_n)/2$ as

$$F(T,n,Y_p^{\rm s})/\Omega = \int_0^n dn'\tilde{\mu}\big(T,n',Y_p^{\rm s}\big). \tag{10}$$

In the quantum statistical approach described above, we relate the EoS to properties of the correlation functions, in particular to the peaks occurring in the A-nucleon spectral function describing the single-nucleon quasiparticle ($A = 1$)

as well as the nuclear quasiparticles ($A \geqslant 2$). Different approaches to these quasiparticle energies can be given by calculating self-energies that reproduce known properties of the nucleonic system. In the following subsections, Secs. II B and II C, we discuss results obtained from a microscopic Hamiltonian approach to nuclear matter. In Sec. III a RMF approach is given that is based on an effective nucleon-meson Lagrangian.

B. Medium modification of single-nucleon properties

The single-particle spectral function contains the single-nucleon quasiparticle contribution, $E_1^{\rm qu}(1) = E_\tau^{\rm qu}(k)$, given in Eq. (4), where τ denotes isospin of particle 1 and k is the momentum. In the effective mass approximation, the single-nucleon quasiparticle dispersion relation reads

$$E_\tau^{\rm qu}(k) = \Delta E_\tau^{\rm SE}(0) + \frac{k^2}{2m_\tau^*} + \mathcal{O}(k^4), \tag{11}$$

where the quasiparticle energies are shifted at zero momentum k by $\Delta E_\tau^{\rm SE}(0)$, and m_τ^* denotes the effective mass of neutrons ($\tau = n$) or protons ($\tau = p$). Both quantities, $\Delta E_\tau^{\rm SE}(0)$ and m_τ^*, are functions of T, n_p, and n_n, characterizing the surrounding matter.

Expressions for the single-nucleon quasiparticle energy $E_\tau^{\rm qu}(k)$ can be given by the Skyrme parametrization [46] or by more sophisticated approaches such as relativistic mean-field approaches [30], see Sec. III, and relativistic Dirac-Brueckner Hartree-Fock [47] calculations. We use the density-dependent RMF approach of Ref. [45] that is designed not only to reproduce known properties of nuclei but also agrees with microscopic calculations in the low-density region. It is expected that this approach gives at present an optimal fit to the quasiparticle energies and is applicable in a large interval of densities and temperatures.

Microscopic calculations are based on a model describing the interaction between the nucleons. To go beyond the mean-field approximation, strong interaction as well as bound-state formation must be taken into account. This can be done in the low-density region where in the nonrelativistic case a T matrix can be introduced. We start from a nonrelativistic Hamiltonian in fermion second quantization,

$$H = \sum_1 E(1) a_1^\dagger a_1 + \frac{1}{2} \sum_{12,1'2'} V(12, 1'2') a_1^\dagger a_2^\dagger a_{2'} a_{1'}, \tag{12}$$

where the kinetic energy is $E(1) = P_1^2/(2m_1)$ and the potential energy contains the matrix element $V(12, 1'2')$ of the nucleon-nucleon interaction.

Because there is no fundamental expression for the nucleon-nucleon interaction, a phenomenological form is assumed to reproduce empirical data such as the nucleon-scattering phase shifts. Different parametrizations are in use. For calculations one can use potentials such as PARIS and BONN or their separable representations [48]. To obtain the empirical parameter values of nuclear matter at saturation density, three-body forces have been introduced in the Hamiltonian (12). In particular, the Argonne AV18/UIX potential [49] has been used to calculate light nuclei [50].

Replacing the two-particle T matrix in the Born approximation with the interaction potential V, we obtain the Hartree-Fock approximation for the energy shift:

$$\Delta E^{\rm HF}(1) = \sum_2 [V(12, 12) - V(12, 21)] f_{1,\tau_2} [E(2) + \Delta E^{\rm HF}(2)]. \tag{13}$$

In this approximation, all correlations in the medium are neglected. The self-energy does not depend on frequency, that is, it is instantaneous in time, with a vanishing imaginary part.

A full Dirac-Brueckner–Hartree-Fock (DBHF) calculation has been performed by Fuchs and Wolter [51] and has been compared with RMF approaches. The relation between the T-matrix approach and the Brueckner G-matrix approach is discussed in detail in Ref. [52]. Extended work has been performed using sophisticated interaction potentials to evaluate the quasiparticle energies in the DBHF approximation (for recent reviews, see Refs. [47,51,53]). There was reasonable agreement between the RMF parametrization of the quasiparticle energies and the DBHF results.

We can assume [18] that the density-dependent RMF parametrization covers a large density region (which is discussed in detail in Sec. III) and that it can be used instead of the above Hartree-Fock shifts to determine the single-nucleon quasiparticle energies. They result as

$$E_{n,p}^{\rm qu}(0) = \sqrt{[m - \Sigma_{n,p}(T, n, \delta)]^2 + k^2} + \Sigma_{n,p}^0(T, n, \delta), \tag{14}$$

where $\Sigma_{n,p}$ and $\Sigma_{n,p}^0$ are the scalar and the time component of the vector self-energy, respectively. In the nonrelativistic limit, the shifts of the quasiparticle energies are

$$\Delta E_{n,p}^{\rm SE}(k) = \Sigma_{n,p}^0(T, n, \delta) - \Sigma_{n,p}(T, n, \delta). \tag{15}$$

The effective masses for neutrons and protons are given by

$$m_{n,p}^* = m - \Sigma_{n,p}(T, n, \delta). \tag{16}$$

Approximations for the functions $\Sigma_{n,p}^0(T, n, \delta)$ and $\Sigma_{n,p}(T, n, \delta)$ are given in the Appendix. These functions reproduce the empirical values for the saturation density $n_{\rm sat} \approx 0.15\,{\rm fm}^{-3}$ and the binding energy per nucleon $B/A \approx -16\,{\rm MeV}$ (see Sec. III D). The effective mass is somewhat smaller than the empirical value $m^* \approx m(1 - 0.17 n/n_{\rm sat})$ for $n < 0.2\,{\rm fm}^{-3}$.

C. Medium modification of cluster properties

Recent progress of the description of clusters in low-density nuclear matter [27,54–56] enables us to evaluate the properties of deuterons, tritons, helions, and helium nuclei in a nonrelativistic microscopic approach, taking the influence of the medium into account.

In addition to the δ-like nucleon quasiparticle contribution, also the contribution of the bound and scattering states can be included in the single-nucleon spectral function by analyzing the imaginary part of $\Sigma(1, z)$. Within a cluster decomposition, A-nucleon T matrices appear in a many-particle approach. These T matrices describe the propagation of the A-nucleon cluster in nuclear matter. In this way, bound states contribute to $n_\tau = n_\tau(T, \tilde{\mu}_n, \tilde{\mu}_p)$ (see Refs. [38,41]). Restricting the

cluster decomposition only to the contribution of two-particle correlations, we obtain the so-called T_2G approximation. In this approximation, the Beth-Uhlenbeck formula is obtained for the EoS, as shown in Refs. [38,41]. In the low-density limit, the propagation of the A-nucleon cluster is determined by the energy eigenvalues of the corresponding nucleus, and the simple EoS (7) results in describing the nuclear statistical equilibrium (NSE).

For nuclei imbedded in nuclear matter, an effective wave equation can be derived [38,56]. The A-particle wave function $\psi_{A\nu K}(1\dots A)$ and the corresponding eigenvalues $E^{\rm qu}_{A,\nu}(K)$ follow from solving the in-medium Schrödinger equation

$$\begin{aligned}\left[E^{\rm qu}(1)+\dots+E^{\rm qu}(A)-E^{\rm qu}_{A,\nu}(K)\right]\psi_{A\nu K}(1\dots A)\\ +\sum_{1'\dots A'}\sum_{i<j}[1-\tilde f(i)-\tilde f(j)]V(ij,i'j')\\ \times\prod_{k\neq i,j}\delta_{kk'}\psi_{A\nu K}(1'\dots A')=0.\end{aligned}\tag{17}$$

This equation contains the effects of the medium in the single-nucleon quasiparticle shifts as well as in the Pauli blocking terms. The A-particle wave function and energy depend on the total momentum K relative to the medium.

The in-medium Fermi distribution function $\tilde f(1)=(\exp\{\beta[E^{\rm qu}(1)-\tilde\mu_1]\}+1)^{-1}$ contains the nonrelativistic effective chemical potential $\tilde\mu_1$, which is determined by the total proton or neutron densities (i.e. including those bound in clusters) calculated in the quasiparticle approximation, $n^{\rm tot}_\tau=\Omega^{-1}\sum_1\tilde f(1)\delta_{\tau_1,\tau}$ for the particles inside the volume Ω. It describes the occupation of the phase space neglecting any correlations in the medium. The solution of the in-medium Schrödinger equation (17) can be obtained in the low-density region by perturbation theory. In particular, the quasiparticle energy of the A-nucleon cluster with Z protons in the ground state follows as

$$\begin{aligned}E^{\rm qu}_{A,\nu}(K)=E^{\rm qu}_{A,Z}(K)=E^{(0)}_{A,Z}+\frac{K^2}{2Am}+\Delta E^{\rm SE}_{A,Z}(K)\\ +\Delta E^{\rm Pauli}_{A,Z}(K)+\Delta E^{\rm Coul}_{A,Z}(K)+\dots,\end{aligned}\tag{18}$$

with various contributions. Besides the cluster binding energy in the vacuum $E^{(0)}_{A,Z}$ and the kinetic term, the self-energy shift $\Delta E^{\rm SE}_{A,Z}(K)$, the Pauli shift $\Delta E^{\rm Pauli}_{A,Z}(K)$, and the Coulomb shift $\Delta E^{\rm Coul}_{A,Z}(K)$ enter. The latter can be evaluated for dense matter in the Wigner-Seitz approximation [57–59]. It is given by

$$\Delta E^{\rm Coul}_{A,Z}(K)=\frac{Z^2}{A^{1/3}}\frac{3}{5}\frac{e^2}{r_0}\left[\frac{3}{2}\left(\frac{2n_p}{n_{\rm sat}}\right)^{\frac{1}{3}}-\frac{n_p}{n_{\rm sat}}\right],\tag{19}$$

with $r_0=1.2$ fm. Because the values of Z are small, this contribution is small as well and disregarded here in the quasiparticle energy (18).

The self-energy contribution to the quasiparticle shift is determined by the contribution of the single-nucleon shift:

$$\Delta E^{\rm SE}_{A,Z}(0)=(A-Z)\Delta E^{\rm SE}_n(0)+Z\Delta E^{\rm SE}_p(0)+\Delta E^{\rm SE,\,eff.mass}_{A,Z}.\tag{20}$$

The contribution to the self-energy shift due to the change of the effective nucleon mass can be calculated from perturbation theory using the unperturbed wave function of the clusters (see Ref. [27]), so that

$$\Delta E^{\rm SE,eff.mass}_{A,Z}=\left(1-\frac{m^*}{m}\right)s_{A,Z}.\tag{21}$$

Values of $s_{A,Z}$ for $\{A,Z\}=\{i\}=\{d,t,h,\alpha\}$ are given in Table I. Inserting the medium-dependent quasiparticle energies in the distribution functions (2) the first two contributions to the quasiparticle shift in Eq. (20) can be included renormalizing the chemical potentials.

The most important effect in the calculation of the abundances of light elements comes from the Pauli blocking terms in Eq. (17) in connection with the interaction potential. This contribution is restricted only to the bound states so that it may lead to the dissolution of the nuclei if the density of nuclear matter increases. The corresponding shift $\Delta E^{\rm Pauli}_{A,Z}(K)$ can be evaluated in perturbation theory provided the interaction potential and the ground-state wave function are known. After angular averaging where in the Fermi functions the mixed scalar product $\vec k\cdot\vec K$ between the total momentum $\vec K$ and the remaining Jacobian coordinates $\vec k$ is neglected, the Pauli blocking shift can be approximated as

$$\Delta E^{\rm Pauli}_{A,Z}(K)\approx\Delta E^{\rm Pauli}_{A,Z}(0)\,\exp\left(-\frac{K^2}{2A^2mT}\right).\tag{22}$$

Avoiding angular averaging, the full solution gives the result up to the order K^2

$$\Delta E^{\rm Pauli}_{A,Z}(K)\approx\Delta E^{\rm Pauli}_{A,Z}(0)\,\exp\left(-\frac{K^2}{g_{A,Z}}\right),\tag{23}$$

with the dispersion that can be calculated from

$$g_i(T,n,Y_p)=\frac{g_{i,1}+g_{i,2}T+h_{i,1}n}{1+h_{i,2}n}.\tag{24}$$

The values for $g_{i,1}$ and $g_{i,2}$ can be calculated from perturbation theory using the unperturbed cluster wave functions; the density corrections $h_{i,1}$ and $h_{i,2}$ are fitted to variational solutions of the in-medium wave equation Eq. (17) for given

TABLE I. Parameters for the cluster binding energy shifts.

Cluster i	s_i (MeV)	$a_{i,1}$ (MeV$^{5/2}$ fm^3)	$a_{i,2}$ (MeV)	$a_{i,3}$	$b_{i,1}$ (fm^3)	$b_{i,2}$ (MeV fm^3)	$g_{i,1}$ (fm^{-2})	$g_{i,2}$ (MeV^{-1} fm^{-2})	$h_{i,1}$ (fm)	$h_{i,2}$ (fm^3)
d	11.147	38 386.4	22.5204	0.2223	1.048	285.7	0.85	0.223	132	17.5
t	24.575	69 516.2	7.49232	–	4.414	43.90	3.20	0.450	37	–
h	20.075	58 442.5	6.07718	–	4.414	43.90	2.638	0.434	43	–
α	49.868	16 4371	10.6701	–	–	–	8.236	0.772	50	–

T, n_p, n_n, and K. Numerical values of the parameters in symmetric nuclear matter ($Y_p = 0.5$) are given in Table I.

The shift of the binding energy of light clusters at zero total momentum that is of first order in density [54,55] has been calculated recently [56]. The light clusters of the deuteron ($d = {}^2$H), the triton ($t = {}^3$H), the helion ($h = {}^3$He), and the α particle (^{4}He) have been considered. The interaction potential and the nucleonic wave function of the few-nucleon system have been fitted to the binding energies and the rms radii of the corresponding nuclei.

With the neutron number $N_i = A_i - Z_i$, it can be written as

$$\Delta E^{\rm Pauli}_{A_i,Z_i}(0; n_p, n_n, T) = -\frac{2}{A_i}[Z_i n_p + N_i n_n]\delta E^{\rm Pauli}_i(T, n), \tag{25}$$

where the temperature dependence and higher density corrections are contained in the functions $\delta E^{\rm Pauli}_i(T, n)$. These functions have been obtained with different approximations for the wave function. In the case of the deuteron, the Jastrow approach leads to a functional form

$$\delta E^{\rm Pauli}_i(T, n) = \frac{a_{i,1}}{T^{3/2}}\left[\frac{1}{\sqrt{y_i}} - \sqrt{\pi}\, a_{i,3} \exp\left(a^2_{i,3} y_i\right) {\rm erfc}(a_{i,3}\sqrt{y_i})\right] \times \frac{1}{1 + [b_{i,1} + b_{i,2}/T]n}, \tag{26}$$

with $y_i = 1 + a_{i,2}/T$. For the other clusters $i = t, h, \alpha$, the Gaussian approach is used, which gives the simple form

$$\delta E^{\rm Pauli}_i(T, n) = \frac{a_{i,1}}{T^{3/2}} \frac{1}{y_i^{3/2}} \frac{1}{1 + [b_{i,1} + b_{i,2}/T]n}. \tag{27}$$

The parameters $a_{i,1}$, $a_{i,2}$, and $a_{i,3}$ are determined by low-density perturbation theory from the unperturbed cluster wave functions. The parameters $b_{i,1}$ and $b_{i,2}$ are density corrections and are fitted to the numerical solution of the in-medium wave equation, Eq. (17), for given $T, n_p, n_n, P = 0$. Values are given in Table I.

Now, the nucleon number densities (7) can be evaluated as in the noninteracting case, with the only difference that the number densities of the particles are calculated with the quasiparticle energies. In the light-cluster–quasiparticle approximation, the total densities of neutrons

$$n^{\rm tot}_n = n_n + \sum_{i=d,t,h,\alpha} N_i n_i \tag{28}$$

and of protons

$$n^{\rm tot}_p = n_p + \sum_{i=d,t,h,\alpha} Z_i n_i \tag{29}$$

contain the densities of the free neutrons and protons, n_n and n_p, respectively, and the contributions from the nucleons bound in the clusters with densities n_i. The state of the system in chemical equilibrium is completely determined by specifying the total nucleon density $n = n^{\rm tot}_n + n^{\rm tot}_p$, the asymmetry δ, and the temperature T as long as no β equilibrium is considered.

This result is an improvement of the NSE and allows for the smooth transition from the low-density limit up to the region of saturation density. The bound-state contributions to the EoS are fading with increasing density because they move as resonances into the continuum of scattering states. This improved NSE, however, does not contain the contribution of scattering states explicitly. For the treatment of continuum states in the two-nucleon case, as well as the evaluation of the second virial coefficient, see Refs. [32,41].

The account of scattering states needs further consideration. Investigations on the two-particle level have been performed and extensively discussed [32,38,41]. We use the Levinson theorem to take the contribution of scattering states into account in the lowest-order approximation. Each bound-state contribution to the density mus be accompanied by a continuum contribution that partly compensates the strength of the bound-state correlations. As a consequence, the total proton and neutron densities are given by

$$n^{\rm tot}_p(T, \tilde\mu_p, \tilde\mu_n) = \frac{1}{\Omega}\sum_{A,\nu,K}^{\rm bound} Z\left\{f_{A,Z}\left[E^{\rm qu}_{A,\nu}(K; T, \tilde\mu_p, \tilde\mu_n)\right] - f_{A,Z}\left[E^{\rm cont}_{A,\nu}(K; T, \tilde\mu_p, \tilde\mu_n)\right]\right\}, \tag{30}$$

$$n^{\rm tot}_n(T, \tilde\mu_p, \tilde\mu_n) = \frac{1}{\Omega}\sum_{A,\nu,K}^{\rm bound} (A - Z)\left\{f_{A,Z}\left[E^{\rm qu}_{A,\nu}(K; T, \tilde\mu_p, \tilde\mu_n)\right] - f_{A,Z}\left[E^{\rm cont}_{A,\nu}(K; T, \tilde\mu_p, \tilde\mu_n)\right]\right\}, \tag{31}$$

with explicit bound and scattering terms. $E^{\rm cont}_{A,\nu}$ denotes the edge of the continuum states that is also determined by the single-nucleon self-energy shifts. These expressions guarantee a smooth behavior when the bound states merge with the continuum of scattering states. The summation over A includes also the contribution of free nucleons, $A = 1$, considered as quasiparticles with the energy dispersion given by the RMF approach.

The summation over K and the subtraction of the continuum contribution is extended only over that region of momentum space where bound states exist. The disappearance of the bound states is caused by the Pauli blocking term; the self-energy contributions to the quasiparticle shifts act on bound as well as on scattering states. Above the so-called Mott density, where the bound states at $K = 0$ disappear, the momentum summation must be extended only over that region $K > K^{\rm Mott}_{A,\nu}(T, n, \delta)$ where the bound-state energy is lower than the continuum of scattering states. The contribution of scattering states is necessary to obtain the second virial coefficient according to the Beth-Uhlenbeck equation (see Refs. [31,41]). This leads also to corrections in comparison with the NSE that accounts only for the bound-state contributions, neglecting all effects of scattering states. These corrections become important at increasing temperatures for weakly bound clusters. Thus, the corrections that lead to the correct second virial coefficient are of importance for the deuteron system when the temperature is comparable or large compared with the binding energy per nucleon. In the calculations for the QS model shown below, the contributions of these continuum correlations have been taken into account.

Solving Eqs. (30) and (31) for given T, $n_p^{\rm tot}$, and $n_n^{\rm tot}$, we find the chemical potentials μ_p and μ_n. After integration, see Eq. (10), the free energy is obtained, and all the other thermodynamic functions are derived from this quantity without any contradictions. Results are given below.

We do not consider the formation of heavy clusters here. This limits the parameter range, $n_n^{\rm tot}$, $n_p^{\rm tot}$, and T, in the phase diagram to that area where the abundances of heavier clusters are small. For a more general approach to the EoS that takes also the contribution of heavier clusters into account, see Ref. [59]. Future work will include the contribution of the heavier clusters.

Further approximations refer to the linear dependence on density of the shifts of binding energies, calculated in perturbation theory. A better treatment will improve these shifts, but it can be shown that the changes are small. The approximation of the uncorrelated medium can be improved considering the cluster mean-field approximation [38,39,56]. Furthermore, the formation of quantum condensates will give additional contributions to the EoS. However, in the region considered here the formation of quantum condensates does not appear. This is in contrast to a recent work employing a quasiparticle gas model [35] where Bose-Einstein condensation of deuterons is observed because the Pauli shift of the deuteron binding energy at high densities is not considered.

III. GENERALIZED RELATIVISTIC MEAN-FIELD MODEL WITH LIGHT CLUSTERS

A main ingredient to construct the low-density EoS is the proper determination of the nucleonic quasiparticle energies that enter the single-nucleon distribution functions, Eqs. (5) and (7), but also the cluster energies via the in-medium Schrödinger equation (17). Recently, realistic values for the nucleon quasiparticle shifts were obtained from sophisticated calculations within Hamiltonian approaches, such as DBHF calculations [51,53]. RMF approaches proved to be very successful in interpreting properties near saturation density (see, e.g., Refs. [18,45]). We extract the single-nucleon quasiparticle shifts from the results of the RMF model with density-dependent couplings and use them in our QS approach. In the following we show how this RMF model can be extended to include light clusters, which are considered as quasiparticles modified by medium effects as obtained in the QS approach. A comparison of the generalized RMF model with the QS model will show distinct differences in the thermodynamical properties that are related to the employed approximations.

In a conventional RMF description [30] of homogeneous and isotropic nuclear matter, nucleons interact by the exchange of mesons where usually isoscalar ω and σ and isovector ρ mesons are included. Neutrons and protons are described by Dirac spinors ψ_i $(i = n, p)$. The mesons are represented by Lorentz vector fields ω_μ and $\vec{\rho}_\mu$ and by a Lorentz scalar field σ. The electromagnetic interaction is not considered in nuclear matter. A possible isovector, Lorentz scalar δ meson, is not included in the present model. The mesons couple minimally to the nucleons. In our approach, nonlinear meson self-interactions are not introduced, but the couplings are assumed to be functionals of the nucleon operator-valued currents to simulate a medium dependence of the interaction.

In the generalized RMF model with light clusters, the ground states of the deuteron ($d = {}^2$H), the triton ($t = {}^3$H), the helion ($h = {}^3$He), and the α particle (^{4}He) are introduced as additional degrees of freedom with the corresponding spin 0 field ϕ_α, spin 1 field ϕ_d^ν, and spin 1/2 fields ψ_i $(i = t, h)$. The clusters are treated as point-like particles and their internal structure is not taken into account. The influence of the medium on the cluster properties is described by density- and temperature-dependent shifts of the binding energies as introduced in the previous section. The Pauli shifts, cf. Eq. (25), are taken from the nonrelativistic calculation neglecting the dependence on the c.m. momentum K of the cluster, whereas this is taken into account in the QS approach. However, the self-energy shift is treated self-consistently in the RMF description in contrast to the QS approach where it enters in parametrized form from an independent model, namely, the RMF model described in this section.

A. Lagrangian density and field equations

In the present approach, the model Lagrangian has the form

$$\begin{aligned}\mathcal{L} = &\sum_{i=n,p,t,h} \bar{\psi}_i\left(\gamma_\mu i D_i^\mu - M_i\right)\psi_i + \frac{1}{2}\left(i D_\alpha^\mu \varphi_\alpha\right)^* \\ &\times \left(i D_{\alpha\mu}\varphi_\alpha\right) - \frac{1}{2}\varphi_\alpha^* M_\alpha^2 \varphi_\alpha + \frac{1}{4}\left(i D_d^\mu \varphi_d^\nu - i D_d^\nu \varphi_d^\mu\right)^* \\ &\times \left(i D_{d\mu}\varphi_{d\nu} - i D_{d\nu}\varphi_{d\mu}\right) - \frac{1}{2}\varphi_d^{\mu *} M_d^2 \varphi_{d\mu} \\ &+ \frac{1}{2}\left(\partial^\mu\sigma\,\partial_\mu\sigma - m_\sigma^2\sigma^2 - \frac{1}{2}G^{\mu\nu}G_{\mu\nu} + m_\omega^2\omega^\mu\omega_\mu \right. \\ &\left. - \frac{1}{2}\vec{H}^{\mu\nu}\cdot\vec{H}_{\mu\nu} + m_\rho^2\vec{\rho}^\mu\cdot\vec{\rho}_\mu\right),\end{aligned} \tag{32}$$

with the field tensors

$$G_{\mu\nu} = \partial_\mu\omega_\nu - \partial_\nu\omega_\mu \qquad \vec{H}_{\mu\nu} = \partial_\mu\vec{\rho}_\nu - \partial_\nu\vec{\rho}_\mu \tag{33}$$

of the Lorentz vector fields. Vectors in isospin space carry an arrow. Nucleons form an isospin doublet with $\tau_3\psi_n = \psi_n$ and $\tau_3\psi_p = -\psi_p$. Similarly, for the triton and helion one has $\tau_3\psi_t = \psi_t$ and $\tau_3\psi_h = -\psi_h$, respectively. Deuterons and α particles are treated as isospin singlets.

The covariant derivative

$$i D_i^\mu = i\partial^\mu - \Gamma_\omega A_i \omega^\mu - \Gamma_\rho |N_i - Z_i| \vec{\tau}\cdot\vec{\rho}^\mu \tag{34}$$

for a particle i contains the interaction with the Lorentz vector mesons with a strength that is determined by the density-dependent couplings Γ_ω, Γ_ρ and the mass (A_i), neutron (N_i), and proton (Z_i) numbers of a particle i. The scalar σ meson with coupling strength Γ_σ appears in the effective mass

$$M_i = m_i - \Gamma_\sigma A_i \sigma - \Delta B_i \tag{35}$$

of a particle i with vacuum rest mass m_i. The vacuum rest mass of a cluster $i = d, t, h, \alpha$ is given by

$$m_i = Z_i m_p + N_i m_n - B_i^0, \tag{36}$$

which defines the vacuum binding energies $B_i^0 > 0$. The medium-dependent Pauli shift ΔB_i appears only for clusters. The couplings $\Gamma_m = \Gamma_m(\varrho)$ $(m = \omega, \sigma, \rho)$ are functionals of the Lorentz scalar density

$$\varrho = \sqrt{J^\mu J_\mu}, \tag{37}$$

which contains the free nucleon current

$$J^\mu = j_p^\mu + j_n^\mu, \tag{38}$$

with $j_i^\mu = \bar{\psi}_i \gamma^\mu \psi_i$. The Pauli shifts of the binding energies were derived in the previous section as the function $\Delta B_i(n_p^{\rm tot}, n_n^{\rm tot}, T)$ depending on the total proton and neutron densities $n_p^{\rm tot}$ and $n_n^{\rm tot}$ and the temperature T. In principle, the densities must be replaced by the corresponding quantities expressed in terms of the field operators of the nucleons and clusters. In the case of the fermions, this poses no problem because the currents of the triton and helion have the same form as the currents of the nucleons. However, for the bosons, the definition of the conserved currents contains the meson fields and the Pauli shifts. A dependence of the Pauli shifts on these currents leads to additional rearrangement contributions that modify the self-energies and require a redefinition of the conserved currents. To avoid these complications, the dependence of the Pauli shifts on the densities is replaced by a dependence on the vector meson fields. In this way the Pauli shifts are treated in an equivalent way as the usual single-particle shifts. In consequence, we replace the dependence on the total densities

$$n_n^{\rm tot} \to n_n^{\rm ps} = \tfrac{1}{2}[\varrho_\omega + \varrho_\rho] \tag{39}$$

and

$$n_p^{\rm tot} \to n_p^{\rm ps} = \tfrac{1}{2}[\varrho_\omega - \varrho_\rho] \tag{40}$$

by pseudodensities $n_n^{\rm ps}$ and $n_p^{\rm ps}$ with the quantities

$$\varrho_\omega = \lambda_\omega \sqrt{\omega^\mu \omega_\mu} \tag{41}$$

and

$$\varrho_\rho = \lambda_\rho \sqrt{\vec{\rho}^\mu \cdot \vec{\rho}_\mu}. \tag{42}$$

The coefficients $\lambda_\omega = m_\omega^2/\,\Gamma_\omega(0)$ and $\lambda_\rho = m_\rho^2/\,\Gamma_\rho(0)$ are defined such that the correct low-density limit is obtained.

The field equations for mesons, nucleons, and clusters are derived from the Lagrangian density in the usual way. They are solved self-consistently in the mean-field approximation where the meson fields are treated as classical fields and sea states of the fermions are not considered. The couplings $\Gamma_m (m = \omega, \sigma, \rho)$ become simple functions of $\varrho = \sqrt{\langle J^\mu \rangle \langle J_\mu \rangle}$, where the brackets $\langle\,\rangle$ indicate the summation over all occupied states of the system. The field equations simplify considerably due to the symmetries of homogeneous and isotropic nuclear matter at rest. The scalar meson field is directly given by

$$\sigma = \frac{\Gamma_\sigma}{m_\sigma^2} n_\sigma, \tag{43}$$

with the source density

$$n_\sigma = \sum_{i=n,p,d,t,h,\alpha} A_i n_i^s \tag{44}$$

that is a sum of the scalar densities $n_i^s = \langle \bar{\psi}_i \psi_i \rangle$ of the fermions $i = n, p, t, h$ and the scalar densities $n_d^s = \langle \varphi_d^\mu M_d \varphi_{d\mu} \rangle$ of the deuteron and $n_\alpha^s = \langle \varphi_\alpha M_\alpha \varphi_\alpha \rangle$ of the α particle. The nonvanishing components of the vector meson fields are

$$\omega_0 = \frac{\Gamma_\omega}{m_\omega^2} n_\omega - \sum_{i=d,t,h,\alpha} \frac{\lambda_\omega}{2m_\omega^2} \left(\frac{\partial \Delta B_i}{\partial n_n^{\rm ps}} + \frac{\partial \Delta B_i}{\partial n_p^{\rm ps}} \right) n_i^s, \tag{45}$$

$$(\vec{\rho}_0)_3 = \frac{\Gamma_\rho}{m_\rho^2} n_\rho - \sum_{i=d,t,h,\alpha} \frac{\lambda_\rho}{2m_\rho^2} \left(\frac{\partial \Delta B_i}{\partial n_n^{\rm ps}} - \frac{\partial \Delta B_i}{\partial n_p^{\rm ps}} \right) n_i^s, \tag{46}$$

with two different source contributions. The regular source densities

$$n_\omega = \sum_{i=n,p,d,t,h,\alpha} A_i n_i \tag{47}$$

$$n_\rho = \sum_{i=n,p,d,t,h,\alpha} (N_i - Z_i) n_i \tag{48}$$

depend on the vector densities $n_i = \langle \bar{\psi}_i \gamma_0 \psi_i \rangle$ of the fermions $i = n, p, t, h$ and on the vector densities of the deuteron

$$\begin{aligned} n_d = \tfrac{1}{2} \langle & (i D_{d0} \varphi_{d\mu} - i D_\mu \varphi_{d0})^* \varphi_d^\mu \\ & + \varphi_d^{\mu *} (i D_{d0} \varphi_{d\mu} - i D_{d\mu} \varphi_{d0}) \rangle \end{aligned} \tag{49}$$

and the α particle

$$n_\alpha = \tfrac{1}{2} \langle (i D_{\alpha 0} \varphi_\alpha)^* \varphi_\alpha + \varphi_\alpha^* (i D_{\alpha 0} \varphi_\alpha) \rangle. \tag{50}$$

The second contribution in Eqs. (45) and (46) with the derivatives of the binding energy shifts is proportional to the scalar densities of the clusters.

The Dirac equation for the spin 1/2 particles $(i = n, p, t, h)$ assumes the form

$$[\gamma^\mu (i \partial_\mu - \Sigma_{i\mu}) - (m_i - \Sigma_i)] \psi_i = 0, \tag{51}$$

with scalar and vector self-energies Σ_i and $\Sigma_{i\mu}$, respectively. The field equations for the α particle and the deuteron are the Klein-Gordon equation

$$-[(i \partial_\mu - \Sigma_{\alpha\mu})(i \partial^\mu - \Sigma_{\alpha\mu}) + (m_\alpha - \Sigma_\alpha)^2] \varphi_\alpha = 0 \tag{52}$$

and the Proca equation

$$\begin{aligned} -(i \partial_\mu - \Sigma_{d\mu}) & \left[\left(i \partial^\mu - \Sigma_d^\mu \right) \varphi_d^\nu - \left(i \partial^\nu - \Sigma_d^\nu \right) \varphi_d^\mu \right] \\ & + (m_d - \Sigma_d)^2 \varphi_d^\nu = 0, \end{aligned} \tag{53}$$

respectively. The scalar self-energies are given by

$$\Sigma_i = \Gamma_\sigma A_i \sigma + \Delta B_i, \tag{54}$$

where the binding energy shift ΔB_i appears only for clusters. The nonvanishing component of the vector self-energy is the zero component

$$\Sigma_{i0} = \Gamma_\omega A_i \omega_0 + \Gamma_\rho (N_i - Z_i) (\vec{\rho}_0)_3 + \Sigma_{i0}^R, \tag{55}$$

with the "rearrangement" contribution

$$\Sigma_{i0}^R = \Gamma_\omega' \omega_0 n_\omega + \Gamma_\rho' (\vec{\rho}_0)_3 n_\rho - \Gamma_\sigma' \sigma n_\sigma \tag{56}$$

that appears only for nucleons. It contains contributions with derivatives $\Gamma_m' = d\Gamma_m/d\varrho$ of the meson-nucleon couplings.

Because the self-energies are momentum independent in homogeneous and isotropic nuclear matter, the field equations of the nucleons and of the clusters are easily solved. The solutions are plane waves with shifted masses and energies as compared to the vacuum solution, that is, nucleons and clusters can be considered as quasiparticles. At finite temperatures T the relevant vector and scalar densities are easily calculated with these solutions by integrating over all momenta with the correct distribution functions. Thus, the vector and scalar densities of the fermions ($i = n, p, t, h$) are given by

$$n_i = g_i \int \frac{d^3k}{(2\pi)^3} [f_i^+(k) - f_i^-(k)] \tag{57}$$

$$n_i^s = g_i \int \frac{d^3k}{(2\pi)^3} \frac{m_i - \Sigma_i}{e_i(k)} [f_i^+(k) + f_i^-(k)], \tag{58}$$

with degeneracy factor $g_i = 2$ and the energy

$$e_i(k) = \sqrt{k^2 + (m_i - \Sigma_i)^2}. \tag{59}$$

The Fermi-Dirac distribution for the particle ($\eta = 1$) and antiparticle ($\eta = -1$) contributions is defined by

$$f_i^\eta(k) = \left\{\exp\left[\eta\beta\left(E_i^\eta - \mu_i\right)\right] + 1\right\}^{-1}, \tag{60}$$

where $\beta = 1/T$ and $E_i^\eta(k) = \Sigma_{i0} + \eta e_i(k)$ is the quasiparticle energy. The (relativistic) chemical potential of a particle i is denoted by μ_i. The densities of the bosons ($i = d, \alpha$) are obtained from

$$n_i = g_i \int \frac{d^3k}{(2\pi)^3} b_i(k) + \tilde{n}_i \tag{61}$$

$$n_i^s = g_i \int \frac{d^3k}{(2\pi)^3} \frac{m_i - \Sigma_i}{e_i(k)} b_i(k) + \tilde{n}_i^s, \tag{62}$$

with the Bose-Einstein distribution

$$b_i(k) = \{\exp[\beta(E_i^+ - \mu_i)] - 1\}^{-1} \tag{63}$$

and degeneracy factors $g_d = 3$ and $g_\alpha = 1$, respectively. A possible contribution to the densities from particles that are condensed in the ground state is denoted by $\tilde{n}_i$ and $\tilde{n}_i^s$. In homogeneous and isotropic matter these two are actually identical. For a system of nucleons and clusters in chemical equilibrium, the (relativistic) chemical potential of a cluster i is determined by

$$\mu_i = N_i\mu_n + Z_i\mu_p. \tag{64}$$

Thus, there are only two independent chemical potentials.

For given total baryon number density n, asymmetry δ, and temperature T, the coupled field equations of the generalized RMF model are solved self-consistently. This procedure yields the chemical potentials of neutrons and protons that determine the densities of all particles. Finally, all thermodynamical quantities, which are specified in the following subsection, can be calculated.

B. Thermodynamical quantities

The energy density ε and the pressure p are derived from the energy-momentum tensor $T^{\mu\nu}$ with the results

$$\begin{aligned}\varepsilon = \langle T^{00}\rangle = &\sum_{i=n,p,t,h} g_i \int \frac{d^3k}{(2\pi)^3} \sum_\eta f_i^\eta e_i(k) \\ &+ \sum_{i=d,\alpha} \left[g_i \int \frac{d^3k}{(2\pi)^3} b_i e_i(k) + \tilde{n}_i \left(m_i - \Sigma_i\right) \right] \\ &+ \Gamma_\omega\omega_0 n_\omega + \Gamma_\rho\rho_0 n_\rho + \frac{1}{2}\left[m_\sigma^2\sigma^2 \right. \\ &\left. - m_\omega^2\omega_0^2 - m_\rho^2\rho_0^2\right]\end{aligned} \tag{65}$$

and

$$\begin{aligned}p = &\frac{1}{3}\sum_{m=1}^{3}\langle T^{mm}\rangle = \frac{1}{3}\sum_{i=n,p,t,h} g_i \int \frac{d^3k}{(2\pi)^3} \sum_\eta f_i^\eta \frac{k^2}{e_i(k)} \\ &+ \frac{1}{3}\sum_{i=d,\alpha} g_i \int \frac{d^3k}{(2\pi)^3} b_i \frac{k^2}{e_i(k)} + (n_n + n_p)[\Gamma'_\omega\omega_0 n_\omega \\ &+ \Gamma'_\rho\rho_0 n_\rho - \Gamma'_\sigma\sigma n_\sigma] - \frac{1}{2}\left[m_\sigma^2\sigma^2 - m_\omega^2\omega_0^2 - m_\rho^2\rho_0^2\right],\end{aligned} \tag{66}$$

with $\rho_0 = (\vec{\rho}_0)_3$. The condensed bosons do not contribute to the pressure but to the energy density. The entropy density s can be extracted from the grand-canonical potential density $\omega(T, \mu_n, \mu_p) = -p$ as $s = -\left(\partial\omega/\partial T\right)|_{\mu_n,\mu_p}$. However, it is more practical to use the thermodynamic relation

$$\varepsilon = Ts - p + \sum_{i=n,p,d,t,h,\alpha} \mu_i n_i \tag{67}$$

corresponding to the Hugenholtz–van-Hove theorem. After partial integration the standard result

$$\begin{aligned}s = -\sum_{i=n,p,t,h} g_i \int \frac{d^3k}{(2\pi)^3} \sum_\eta \left[f_i^\eta \ln f_i^\eta \right. \\ \left. + \left(1 - f_i^\eta\right)\ln\left(1 - f_i^\eta\right)\right] - \sum_{i=d,\alpha} g_i \int \frac{d^3k}{(2\pi)^3} \\ \times [b_i \ln b_i - (1 + b_i)\ln(1 + b_i)]\end{aligned} \tag{68}$$

is obtained. The thermodynamical pressure

$$p = n^2 \left.\frac{\partial}{\partial n}\left(\frac{f}{n}\right)\right|_{T,\delta} \tag{69}$$

calculated from the free energy density $f = \varepsilon - Ts$ is identical to the pressure (66) in the field theoretical approach. Because the energy density in the RMF model contains the contribution of the rest mass of the particles, it is convenient to define the internal energy per nucleon as

$$E_A(n, \delta, T) = \frac{1}{n}\left[\varepsilon(n, \delta, T) - n_n^{\text{tot}} m_n - n_p^{\text{tot}} m_p\right] \tag{70}$$

and correspondingly the free energy per nucleon as

$$F_A(n, \delta, T) = E_A - T\frac{s}{n}, \tag{71}$$

where the rest mass has been subtracted. We emphasize that both the generalized RMF model and the QS approach are thermodynamically consistent.

C. Dissolution of clusters

In the generalized RMF approach, the quasiparticle energy shift of the clusters contains the self-energy shift due to the mean fields of the mesons. The effective-mass shift is already included in the relativistic approach and the Coulomb shift is neglected. For the binding energy shift ΔB_i only the effect of the Pauli blocking is considered. The dependence of the Pauli shift on the cluster momentum relative to the medium is neglected because the introduction of a momentum dependence in the RMF Lagrangian is nontrivial [45]. With increasing density of the medium, the linear approximation of the Pauli shift (25) in the densities is not sufficient and higher-order terms must be considered. In the present RMF calculation, an empirical quadratic form

$$\Delta B_i\left(n_p^{\rm tot}, n_n^{\rm tot}, T\right) = -\tilde{n}_i\left[1 + \frac{\tilde{n}_i}{2\tilde{n}_i^0(T)}\right]\delta B_i(T) \qquad (72)$$

is used, where the abbreviation

$$\tilde{n}_i = \frac{2}{A_i}\left[Z_i n_p^{\rm tot} + N_i n_n^{\rm tot}\right] \qquad (73)$$

and the density scale

$$\tilde{n}_i^0(T) = \frac{B_i^0}{\delta B_i(T)} \qquad (74)$$

for the dissolution of the cluster i with the vacuum binding energy B_i^0 are introduced. The quantity $\delta B_i(T)$ is given by $\delta E_i^{\rm Pauli}(T, 0)$ in Eq. (26) for deuterons and in Eq. (27) for the other clusters. In the limit $T \to 0$ the shifts and their derivatives remain finite for all clusters.

The total binding energy of a cluster i is the sum $B_i = B_i^0 + \Delta B_i$ of the experimental binding energy B_i^0 in the vacuum [60] and the binding energy shift ΔB_i that in general depends on the c.m. momentum K (see Sec. II C). The dependence of the cluster binding energies on the total nucleon density $n = n_n^{\rm tot} + n_p^{\rm tot}$ of the medium is depicted for symmetric nuclear matter in Fig. 1 for various temperatures T and clusters at rest. For $n \to 0$ the experimental binding energy is recovered. The density where a cluster becomes unbound, that is, $B_i = 0$, increases with increasing temperature. This behavior is expected because the Pauli blocking of states is less effective at higher temperatures. Note that both free nucleons and nucleons bound in clusters are relevant for the Pauli principle occupying phase space in momentum representation. In principle, this is not described by a Fermi distribution but by the bound-state wave functions. A more exact theory taking this into account is given by the cluster mean-field approximation [56], which, however, is very complex and has not been solved in general so far. Here we use the approximation of an effective Fermi distribution with an effective chemical potential that includes both free and bound-state nucleons, as discussed following Eq. (17). It is clearly seen that the weakly bound deuteron dissolves in the medium at densities much lower than those of the more tightly bound α particle.

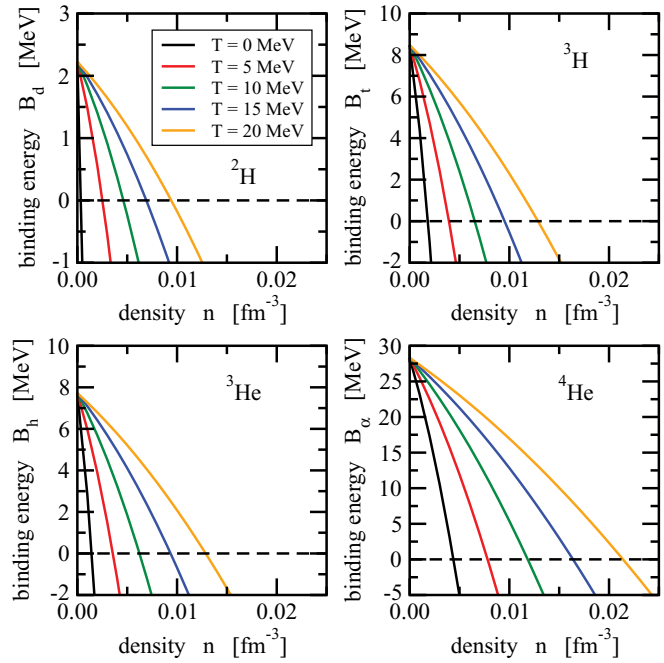

FIG. 1. (Color online) Change of the binding energy $B_i = B_i^0 + \Delta B_i$ of the clusters $i = d, t, h, \alpha$ at rest in symmetric nuclear matter due to the binding energy shift ΔB_i as used in the generalized RMF model as a function of the total nucleon density $n = n_n^{\rm tot} + n_p^{\rm tot}$ of the medium for various temperatures T.

The quadratic form (72) of the binding energy shift ΔB_i predicts a transition of the cluster bound state to the continuum at a transition density of $\tilde{n}_i^t(T) = (\sqrt{3} - 1)\tilde{n}_i^0(T)$ where the cluster binding energy B_i becomes zero; that is, there are only scattering correlations remaining and the energy corresponds to that of a resonance. In the case of the triton, the helion, and the α particle, the resonance energy rapidly moves to larger energies in the continuum with increasing density leading to a strong suppression of the cluster fractions. In contrast, the deuteron-like resonance stays closer to the threshold causing a much weaker suppression of two-particle correlations at high densities. The change of the binding energy from positive to negative values allows one to describe a continuous suppression of the cluster fraction with increasing density. A simple neglection of the cluster contribution to the EoS as soon the energy crosses zero would lead to an unphysical jump in the cluster density and the thermodynamical properties. In the QS model, the bound-state contributions are rapidly canceled by the continuum contributions, Eqs. (30) and (31) leading to a more rapid suppression also of the deuteron correlations. The differences in the continuum correlations will be seen to have large effects in the comparison of the results from the RMF and QS models.

D. Model parameters

The generalized RMF model contains several parameters: the masses of the particles, the couplings and binding-energy shifts with their specific functional dependence on densities and temperature. In the present approach, experimental

TABLE II. Masses of the nucleons and mesons in the relativistic mean-field model.

Particle i	Neutron	Proton	ω meson	σ meson	ρ meson
m_i (MeV)	939.56536	938.27203	783	546.212459	763

neutron and proton masses m_n and m_p are used instead of an average nucleon mass $m_{\rm nuc} = (m_n + m_p)/2$. With the experimental binding energies B_i^0 in the vacuum from Ref. [60] the masses (36) of the clusters are also fixed. For the masses of the ω- and ρ-meson standard values of previous RMF models are assumed. The mass of the σ meson is determined from a fit of the RMF parameters to properties of finite nuclei (see below). The numerical values of the nucleon and meson masses are given in Table II.

The functional dependence of the couplings on the density is described by

$$\Gamma_i(n) = \Gamma_i(n_{\rm sat}) f_i(x), \tag{75}$$

with $x = n/n_{\rm sat}$ where a rational function

$$f_i(x) = a_i \frac{1 + b_i(x + d_i)^2}{1 + c_i(x + d_i)^2} \tag{76}$$

is used for the isoscalar mesons $i = \omega, \sigma$ and an exponential function

$$f_i(x) = \exp[-a_i(x - 1)] \tag{77}$$

for the isovector meson $i = \rho$. To reduce the number of independent parameters the conditions $f_i(1) = 1$ and $f_i''(0) = 0$ are imposed on the rational function. These functions were introduced in Ref. [45] and are now widely used in RMF models with density-dependent couplings. The saturation density $n_{\rm sat}$, the mass of the σ meson m_σ, the couplings $\Gamma_i(n_{\rm sat})$, and the coefficients a_i, b_i, c_i, and d_i are found by fitting the properties of finite nuclei (binding energies, spin-orbit splittings, charge and diffraction radii, surface thicknesses, and the neutron skin thickness of ^{208}Pb) in the same way as for the parametrization DD in Ref. [45]. In total, there are ten independent parameters in the fit. Numerical values of the coupling parameters can be found in Table III. This new parametrization is called DD2 because it is a modification of the set DD where the only difference is the use of experimental nucleon masses.

On the basis of this fit, the saturation density of symmetric nuclear matter at zero temperature is obtained as $n_{\rm sat} = 0.149065\,{\rm fm}^{-3}$ with a binding energy per nucleon of -16.02 MeV. The incompressibility turns out to be $K_\infty = 242.7$ MeV with a derivative $K' = -529.8$ MeV. See Refs. [18,45] for the definition of these quantities. These values are very reasonable and close to the results of other modern RMF parametrizations. The large negative value of K' is a result of the fit to the surface properties of nuclei and leads a rather stiff EoS for symmetric nuclear matter at high densities. The small effective Dirac mass at saturation of $0.5625 m_{\rm nuc}$ is required to get a good description of the spin-orbit splittings. This corresponds to an effective Landau mass of $m^* = 0.6255 m_{\rm nuc}$.

TABLE III. Parameters of the couplings in the relativistic mean-field model.

Meson i	$\Gamma_i(n_{\rm sat})$	a_i	b_i	c_i	d_i
ω	13.342362	1.369718	0.496475	0.817753	0.638452
σ	10.686681	1.357630	0.634442	1.005358	0.575810
ρ	3.626940	0.518903			

The value and the density dependence of the symmetry energy near the nuclear saturation density $n_{\rm sat}$ are usually characterized by the quantities $J = E_{\rm sym}(n_{\rm sat}, 0, 0)$ and the slope parameter $L = 3d E_{\rm sym}/dn|_{n=n_{\rm sat},T=0}$. With the parametrization of the present RMF model, the values $J = 32.73$ MeV and $L = 57.94$ MeV are found. The obtained symmetry energy at saturation J is fully consistent with all modern RMF parametrizations and expectations. The rather small slope coefficient L is a consequence of fitting the neutron skin thickness of ^{208}Pb that is not known precisely so far. Similar low values for L are found in other contemporary RMF parametrizations with density-dependent couplings or with extended nonlinear meson self-interactions. Older nonlinear RMF models were not able to give a reasonable value of the neutron skin thickness with values for L in excess of 100 MeV. They displayed a much stiffer symmetry energy because of a restricted form for the isospin dependence of the interaction. The symmetry energy of nuclear matter parameters at subsaturation densities is one of the central results of this work and is discussed in Sec. VI.

IV. PROPERTIES OF SYMMETRIC NUCLEAR MATTER WITH LIGHT CLUSTERS

The appearance of light clusters in nuclear matter at densities below saturation affects the composition and the thermodynamical properties of the system. In this section we compare the results of the QS approach with the generalized RMF in reference to the NSE model, which gives the correct behavior in the limit of small densities. We will start to discuss the composition of the system, which shows most directly the differences of the models. In all figures in this section we consider isothermes in symmetric nuclear matter as a function of the total baryon density for temperatures between 2 and 20 MeV in steps of 2 MeV keeping the same color code. This representation immediately allows one to study the systematic evolution of the various properties.

A. Composition

We start to discuss the composition of the system, that is, the fractions $X_i = A_i n_i/n$ of the various particle species i as calculated in the RMF and the QS models. We first describe the results and then attempt to give an explanation of the differences between the models at the end of the subsection.

In Fig. 2 the density dependence of the free proton fraction, that is, of protons not bound in a cluster, is shown for

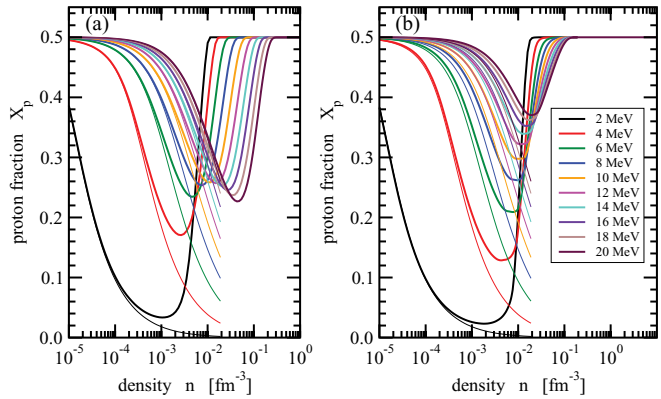

FIG. 2. (Color online) Proton fraction X_p in symmetric nuclear matter as a function of the total density n for various temperatures T in the generalized RMF model (a) and the QS approach (b) with light clusters (thick solid lines). The results of the NSE calculation with light clusters are denoted by thin solid lines for low densities.

different temperatures in symmetric nuclear matter (which in this case is nearly identical to the neutron fraction). The two approaches are compared to the NSE model up to densities $n < 2 \times 10^{-2}\,\mathrm{fm}^{-3}$. For finite temperatures T the free proton fraction in symmetric nuclear matter always approaches the value 0.5 for $n \to 0\,\mathrm{fm}^{-3}$. It first decreases with increasing densities because of the formation of clusters, but then increases again because the clusters dissolve at higher densities. Eventually the system becomes homogeneous again, and the nucleon fractions attain the value 0.5. For densities below $n \sim 10^{-4}\,\mathrm{fm}^{-3}$ the fraction of free protons in both models is very well described by the NSE result because here mean-field effects and changes of the cluster properties are practically negligible. With increasing density, the NSE proton fraction approaches zero asymptotically irrespective of the temperature; that is, all protons are predicted to be bound in clusters. This unphysical result does not occur in both the RMF and QS approaches. Instead, the clusters dissolve at high densities leading to free protons and neutrons at high densities; that is, the correct limit is obtained.

The two approaches, RMF and QS, generally show a similar behavior. However, in the transition region where the clusters dissolve, there are significant differences, which are more pronounced at high temperatures. In the QS approach the minimum of the free proton fraction increases with the temperature monotonously, and the minimum position is slightly shifted to higher values in density but stays close to $10^{-2}\,\mathrm{fm}^{-3}$. Essentially all protons are free at saturation density independent of temperature. In the RMF model the behavior at temperatures above $\approx$8 MeV is different. The minimum of X_p starts to decrease again and the minimum position moves considerably to higher densities with increasing temperature, such that the model predicts that some protons are still bound in clusters even at saturation density.

The information on the fractions of the different light clusters, deuteron to ^{4}He, is shown in Fig. 3 for the RMF model and in Fig. 4 for the QS model, again in comparison with NSE. At zero temperature and density the cluster fractions are simply determined by the binding energies. Thus in symmetric nuclear

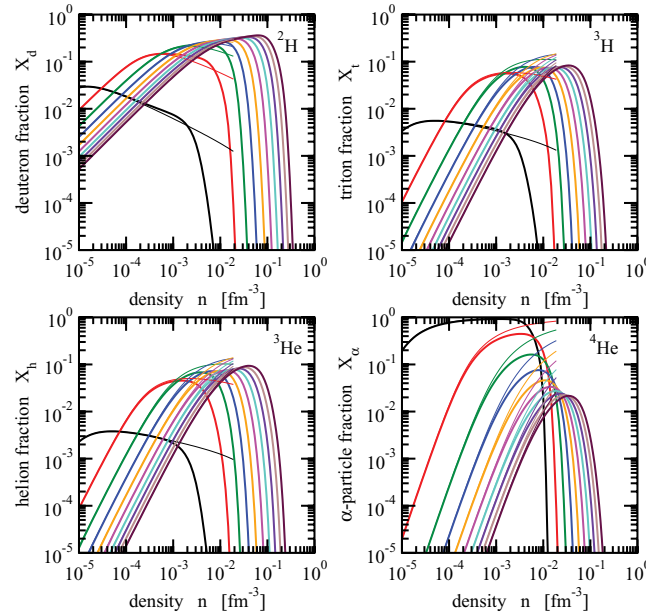

FIG. 3. (Color online) Cluster fractions X_i in symmetric nuclear matter as a function of the total density n for various temperatures T in the generalized RMF model (thick solid lines). The results of the NSE calculation with light clusters are denoted by thin solid lines for low densities. See Fig. 2 for the color code.

matter all nucleons are bound in α particles. With increasing temperature the cluster fractions show the complementary behavior compared to the free nucleon fractions, discussed previously. At low densities and higher temperatures all cluster fractions are small, decreasing with temperature but increasing

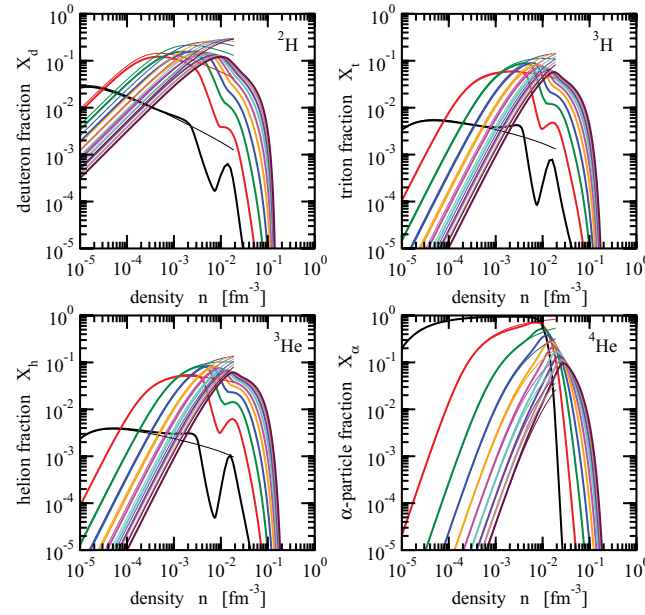

FIG. 4. (Color online) Cluster fractions X_i in symmetric nuclear matter as a function of the total density n for various temperatures T in the QS approach (thick solid lines). The result of the NSE calculation with light clusters is denoted by thin solid lines for low densities. See Fig. 2 for the color code.

with density. For a fixed temperature first the deuteron appears, then the three-body bound states, and finally the α particle. The distribution between the clusters changes with increasing density of the medium such that correlations between more and more nucleons become important. As a consequence, the fractions of the lighter clusters decrease whereas the α-particle fraction still increases. In the QS model (but not in the RMF model) at higher densities the more strongly bound α particles are formed more frequently than deuterons. The same trend is observed for the NSE calculation. However, for densities beyond nuclear saturation, the NSE model predicts that all nucleons in symmetric nuclear matter would be bound in clusters, which again is unphysical because in this model the medium modification and the eventual disappearance of the clusters is not taken into account.

Again there are significant differences in the two approaches. In the RMF model the cluster fractions along isothermes rise and fall monotonously with a single maximum. In general they stay below the fractions predicted by the NSE calculation, because the clusters are less bound inside the medium. In the QS approach, however, at lower temperatures, the fractions of deuterons, tritons, and helions exhibit a sudden drop around densities of 10^{-2} fm^{-3}, which is accompanied by an increase in the α-particle fraction as compared to the NSE result. Generally, the range of densities where the clusters disappear is more confined in the QS model relative to the RMF model.

Many of the differences in the behavior of the models can be traced back to the different treatments of the deuteron correlations. The QS approach takes the continuum contributions explicitly into account, which effectively reduces the strength of the two-body correlations, as is, for example, seen in Eqs. (30) and (31). In the RMF model, on the other hand, the deuteron correlations are represented by a single state that slowly moves to higher energies in the continuum, and thus two-body correlations are overestimated. Also in the NSE model, the deuteron correlations are overestimated, because there is no continuum contribution. This has a strong effect on the deuteron fraction and—in competition—also on the fractions of nucleons and other clusters. We see that in the RMF model the deuteron fractions at higher densities are generally larger than those in the QS model, as seen by comparing the upper-left panels of Figs. 3 and 4. This, in turn, has a strong effect on the α fractions, which are much lower in the RMF model as seen in the lower-right panels of these figures, but also leads to the decrease of the free nucleon fraction at higher densities, as seen in Fig. 2. These effects can also be seen in the comparison with the NSE limit, where they lead to larger deuteron fractions relative to the QS model. Only at temperatures smaller than the deuteron binding energy is the bound state the dominating two-body correlation. A similar effect occurs in the virial description of matter at low densities that is encoded in the temperature dependence of the second virial coefficient. For heavier clusters the influence of the continuum on the fractions is much less pronounced as a result of their larger binding energies.

As we remarked above, the QS model shows a particularly enhanced α-particle fraction at the higher densities, as seen in the increase above the NSE limit at densities around $n \sim 10^{-2}$ fm^{-3} in Fig. 4. This has much of the appearance of an onset of an α-particle condensation. As a consequence, the fractions of the other clusters show a dip around this density, and there are also consequences in the thermodynamical quantities, as seen in the next subsection. All these effects are not present in the RMF model. However, mean-field contributions from the rather substantial cluster fractions in this density range are not taken into account in the QS model, the effect of which needs to be further investigated. It is important to note that the α particle is usually not the most frequent cluster and that there are substantial contributions from the deuteron, the triton, and the helion at intermediate densities and temperatures that are not considered in the EoS of Lattimer and Swesty [28] or Shen *et al.* [29]. Furthermore, the excluded-volume mechanism to suppress the formation of clusters at high densities does not take into account any temperature dependence in this process, which is clearly present in our more microscopic models.

B. Thermodynamical quantities

In this subsection we discuss the thermodynamical quantities for symmetric nuclear matter. The essential effects of the formation of clusters in the various models are given by the pressure p as a function of the total baryon number density density n. For a better representation, we depict in Fig. 5 the ratio p/n as a function of n. The left and right panels of the figure show the results of the RMF and the QS models, respectively, with thick lines. The thin lines in both panels represent a NSE calculation with neutrons, protons, and the light clusters d, t, h, and α. They are shown only for densities below 2×10^{-2} fm^{-3} because the contribution of heavier clusters can be substantial at higher densities, at least for low temperatures, and the NSE becomes unrealistic.

At very low densities, all models approach the ideal gas limit with $p/n = T$ because the cluster fraction is very small and nuclear matter is composed primarily of neutrons and

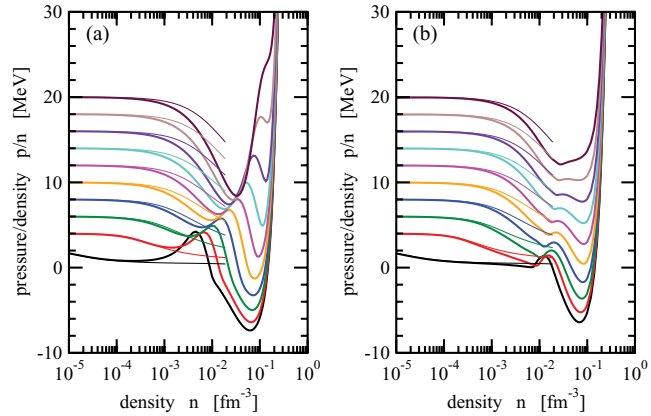

FIG. 5. (Color online) Ratio pressure over density p/n of symmetric nuclear matter as a function of the total density n for various temperatures T in the generalized RMF model (a) and the QS approach (b) with light clusters (thick solid lines). The results of the NSE calculation with light clusters are denoted by thin solid lines for low densities. See Fig. 2 for the color code.

protons (see Sec. IV A). Relativistic and mean-field effects are not important here. With increasing density the NSE calculation exhibits a reduction of the pressure relative to the ideal gas that is caused by the formation of light clusters. Both the RMF and the QS models follow this trend but there are considerable differences. The QS result stays closer to the NSE calculation whereas RMF shows a deviation already at lower densities around 10^{-3} fm. However, both models predict a stronger decrease of the pressure stronger than the NSE, because at these densities the changes of the cluster properties and the mean-field effects are already effective. An exception is seen for the RMF approach at temperatures below approximately 6 MeV where it shows an increase relative to the NSE.

In the density range from 10^{-2} to 2×10^{-1} fm^{-3} the ratio p/n displays considerable structure and passes through at least one minimum, eventually with negative pressure, before it rises sharply for densities above nuclear saturation ($p/n = 0$) and the matter becomes very incompressible. In this region, we observed the most pronounced differences in the behavior of the RMF and QS models with respect to the composition in Sec. IV A. They are generated partly by differences in the description of the cluster correlations and partly by a different treatment of the mean-field effects. In the QS approach, the strengths of the mean fields and thus the quasiparticle energies and mass shifts are independent of the composition of the system because they are taken in parametrized form from the RMF calculation without clusters. In contrast, in the RMF approach the additional contributions in the source terms of the meson fields, see Eqs. (45) and (46), depend on the cluster densities. They describe the back reaction of the cluster formation on the medium (apart from the contribution of the bound nucleons) and are inevitable for the thermodynamical consistency of this model. In the density region where the cluster fraction is substantial, the additional terms lead to a sizable modification of the vector meson fields. In the density range around $n \sim 10^{-2}$ fm^{-3} the pressure is lower in the QS model relative to the RMF model. This correlates with increased α formation (α "condensation") in this model relative to RMF, as is seen in Fig. 4.

The relativistic baryon chemical potentials $\mu = (\mu_p + \mu_n)/2$ of the RMF and the QS approaches are displayed in Fig. 6 in comparision with the NSE calculation. They reflect the behavior observed for the pressure of the various models. At very low densities, the three calculations agree with each other and the ideal gas dependence of the chemical potential $\mu = m + T \ln(n\lambda^3/4)$ on temperature and density. With increasing density, the chemical potential of both the RMF and QS calculations are below the NSE results, except for the RMF model at low temperatures as already seen for the pressure. Here, the chemical potential rises above the NSE result with increasing density and a pronounced maximum occurs. In the QS model, the chemical potential generally stays below the NSE result. Deviations from the NSE predictions appear already at lower densities in the RMF model relative to the QS model. In general, however, the differences between the two approaches are less obvious in the chemical potential than in the pressure. In both models the low-density and the high-density limits are correctly described.

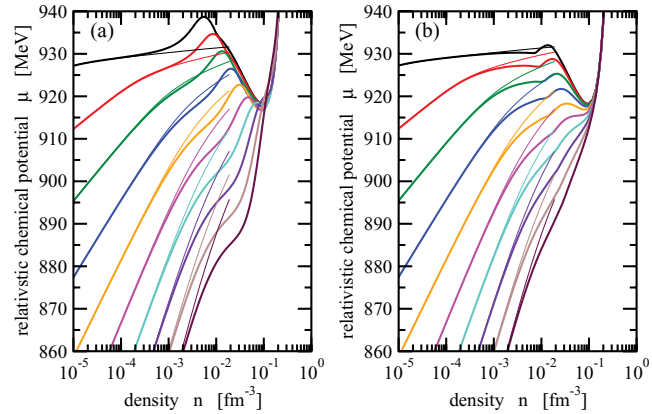

FIG. 6. (Color online) Relativistic baryon chemical potential $\mu = (\mu_p + \mu_n)/2$ of symmetric nuclear matter as a function of the total density n for various temperatures T in the generalized RMF model (a) and the QS approach (b) with light clusters (thick solid lines). The results of the NSE calculation with light clusters are denoted by thin solid lines for low densities. See Fig. 2 for the color code.

The density dependence of the free energy per nucleon F_A, Eq. (71), is shown in Fig. 7 and closely follows the density dependence of the chemical potential. In the QS approach, F_A is obtained by a simple direct integration of the chemical potential, cf. Eq. (10). Both models agree perfectly with the NSE result for densities below 10^{-4} fm^{-3}. At the nuclear saturation density, the free binding energy per nucleon approaches the local minumum at -16 MeV in the limit $T \to 0$ MeV as expected.

The results for the internal energy per nucleon E_A are depicted in Fig. 8. Here the differences between the RMF and the QS results are less pronounced than in the chemical potential μ or the free binding energy per nucleon F_A. In contrast to the latter quantities, E_A increases with temperature at a given density. For $n \to 0$ the classical limit $E_A \to 3T/2$ of an ideal gas is approached. Slight deviations stem from the use of relativistic dispersion relations.

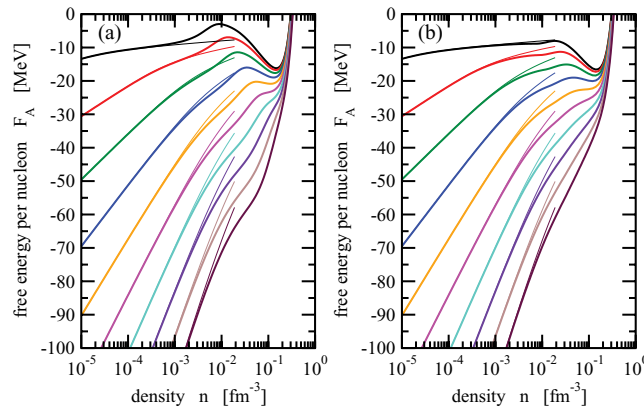

FIG. 7. (Color online) Free energy per nucleon F_A of symmetric nuclear matter as a function of the total density n for various temperatures T in the generalized RMF model (a) and the QS approach (b) with light clusters (thick solid lines). The results of the NSE calculation with light clusters are denoted by thin solid lines for low densities. See Fig. 2 for the color code.

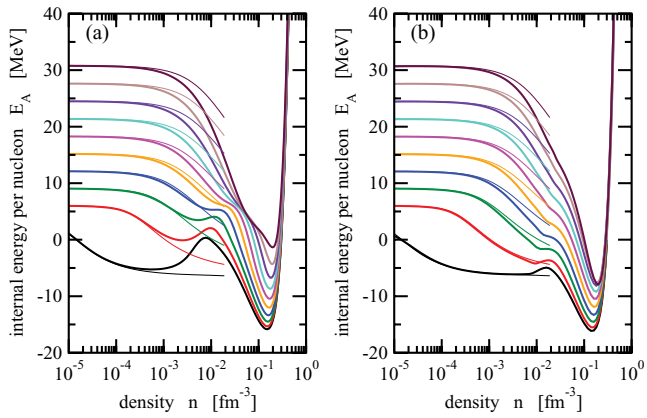

FIG. 8. (Color online) Internal energy per nucleon E_A of symmetric nuclear matter as a function of the total density n for various temperatures T in the generalized RMF model (a) and the QS approach (b) with light clusters (thick solid lines). The results of the NSE calculation with light clusters are denoted by thin solid lines for low densities. See Fig. 2 for the color code.

The entropy per nucleon $S_A = s/n$, shown in Fig. 9, generally decreases monotonously with increasing density n except for a small range in density at low temperatures when the light clusters suddenly dissolve in the medium. At low densities the entropy per nucleon in the RMF and QS models approaches the NSE result and at very low densities, a dependence $S_A \propto -\ln(n) + \text{const.}$ is found consistent with the behavior of an ideal gas. The occurrence of clusters is found to lead to a reduction of the entropy per nucleon as compared to pure neutron-proton matter.

V. LIQUID-GAS PHASE TRANSITION

In a system of given total neutron and protons number densities, n_n^{tot} and n_p^{tot}, and temperature T, the corresponding thermodynamical potential, that is, the free energy density

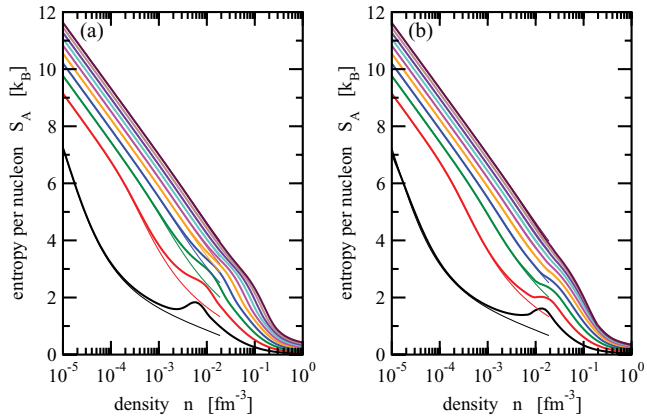

FIG. 9. (Color online) Entropy per nucleon S_A of symmetric nuclear matter as a function of the total density n for various temperatures T in the generalized RMF model (a) and the QS approach (b) with light clusters (thick solid lines). The results of the NSE calculation with light clusters are denoted by thin solid lines for low densities. See Fig. 2 for the color code.

$f(n_n^{\text{tot}}, n_p^{\text{tot}}, T)$, should be minimized. However, this procedure does not necessarily give the correct equilibrium state. Thermodynamic laws require that the free energy density is a convex function in the variables n_n^{tot}, n_p^{tot}, and T to assure the stability of the system. This condition leads to the occurrence of phase transitions. The coexistence region of different phases in thermodynamical equilibrium is separated from the region of a single phase by the so-called binodal surface. It can be obtained for a given temperature by a general Gibbs construction where the values of the intensive variables pressure p and the chemical potentials of protons μ_p and neutrons μ_n in the two phases must be identical (see, for example, Refs [61,62]). Thus, the binodal surface is found from a global criterion in contrast to the spinodal surface that defines the boundary of local instability of the system, which occurs, for example, when the compressibilities of the system become negative. In general, the spinodal is enclosed by the binodal and both become identical along critical lines. In the case of symmetric nuclear matter, the problem becomes one-dimensional and a usual Maxwell construction for the phase transition is sufficient with constant pressure p and baryon chemical potential μ for densities inside the coexistence region. In the general case of asymmetric matter, the pressure and chemical potentials do not stay constant. In addition, the low-density phase has an isospin asymmetry larger than that of the coexisting high-density phase.

Nuclear matter as considered here is an idealized physical system where the Coulomb interaction is neglected and charge neutrality is not demanded. The phase transition boundary as constructed by the aforementioned standard procedure only gives a first indication of where the formation of inhomogeneities and heavy nuclei occurs. In more realistic calculations with Coulomb interaction the system must be globally charge neutral and at least the contribution of electrons must be considered, for example, in applications of the EoS to astrophysics. We do not follow up on this issue in the present work. For references to work in this direction, see our discussion of pasta phases in the Introduction.

The results for the pressure p, Fig. 5, and the baryon chemical potential μ, Fig. 6, allow one to construct the phase transition in symmetric nuclear matter from the gas phase with nucleons and light clusters at small densities to the liquid phase of pure nucleon matter at high densities. In the following we consider the example of the RMF model. In Fig. 10 the pressure p and the chemical potential μ with phase transition are shown for the cases without and with light clusters. Inside the coexistence region of the two phases pressure and chemical potential stay constant as characteristic for a Maxwell construction. As the temperature approaches zero, the density range of this region becomes larger with the limits $p \to 0\,\text{MeV fm}^{-3}$ and $\mu \to m - 16\,\text{MeV}$. The differences between the calculations without and with clusters increase at higher temperatures with a larger coexistence pressure in the latter case. Finally, the critical temperature is reached beyond which no phase transition occurs any more.

At low temperatures the binodal line at the lower boundary of the coexistence region is reached already at very small densities. At this point the cluster fraction is still rather small, and, consequently, the appearance of clusters has little effect on

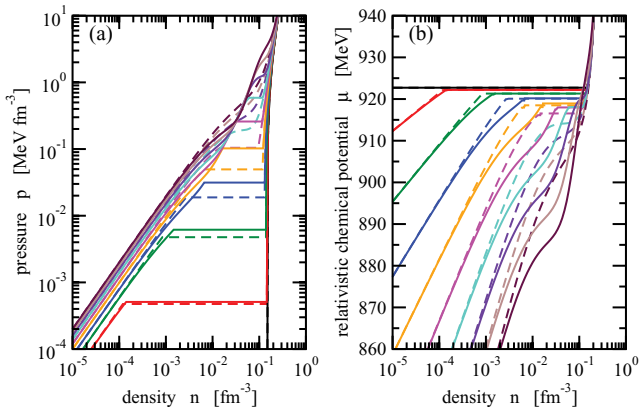

FIG. 10. (Color online) Pressure (a) and relativistic baryon chemical potential (b) of symmetric nuclear matter as a function of the baryon number density in the generalized RMF model with clusters (solid lines) and without clusters (dashed line) taking the phase transition into account. See Fig. 2 for the color code.

the determination of the phase boundary for low temperatures. Larger effects of the clusters on the phase transition are observed only at higher temperatures where the cluster fraction at the lower density boundary reaches larger values. The binodal on the high-density side of the phase coexistence region is hardly affected when clusters are considered in the calculation because here the matter is essentially composed of free nucleons.

Results such as in Fig. 10 can be used to extract the binodal line enclosing the phase coexistence region in the p-n diagram and the phase transition line in the T-μ diagram. These are shown in the left and right panels of Fig. 11, respectively, for the RMF model without and with clusters and the QS approach. The occurrence of light clusters in the system narrows the width of the coexistence region and shifts the maximum to a higher density and larger pressure in the generalized RMF

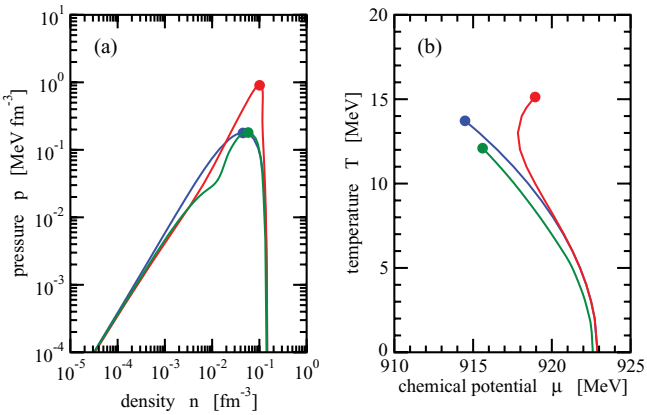

FIG. 11. (Color online) Binodal line enclosing the liquid-gas coexistence region in the pressure-density diagram (a) and phase transition line in the temperature-chemical potential diagram (b) for symmetric nuclear matter in the RMF model without light clusters (blue lines), with light clusters (red lines), and in the QS approach (green lines). The corresponding critical points are denoted by solid circles.

model as compared to the calculation without clusters. In the RMF model the critical temperature T_c increases from 13.72 MeV without clusters to 15.12 MeV with clusters. The corresponding values of the critical density n_c are 0.0452 and 0.1018 fm^{-3} and of the critical pressure p_c are 0.1781 and 0.9029 MeV fm^{-3}, respectively. Thus, in the RMF model the position of the critical point shifts rather drastically when light clusters are considered. There is also a marked effect on the phase transition line in the T-μ diagram. In RMF without clusters, the chemical potential decreases monotonously with increasing temperature until it reaches the critial point at a critical chemical potential of $\mu_c = 914.48$ MeV. At low temperatures the phase transition line with clusters follows closely the line without clusters. However, toward the critical point the transition line with light clusters has as S shape. At temperatures T above $\approx$8 MeV the curve finally bends to higher chemical potentials ending at the critical point with $\mu_c = 918.9$ MeV.

In the QS approach a very different trend is found. The binodal line exhibits a characteristic dip on the low-density side that is related to the enhancement of the α-particle fraction (cf. Fig. 4). The critical point moves to a smaller temperature of $T_c = 12.1$ MeV and a slightly higher chemical potential of $\mu_c = 915.61$ MeV as compared to the RMF calculation without clusters. The critical pressure hardly changes. The observed differences between the RMF and the QS approaches are again related to the fact that many-body correlations at high temperatures, especially of the deuteron, are overestimated in the former. The behavior of the RMF approach must be considered unphysical in this respect, because one would expect that correlations decrease the chemical potential and the pressure of the phase transition. In an improved version of the generalized RMF approach that takes the continuum contributions explicitly into account, it is expected that the critical point moves to lower temperatures.

VI. SYMMETRY ENERGY

The internal energy per nucleon E_A of asymmetric nuclear matter, as defined in Eq. (70), can be expanded for given density n and temperature T in powers of the asymmetry δ:

$$E_A(n, \delta, T) = E_A(n, 0, T) + E_{\rm sym}(n, T)\delta^2 + \ldots . \quad (78)$$

The symmetry energy is the coefficient of the first term in the expansion that depends on the asymmetry δ quadratically. Thus, it is defined as the second derivative

$$E_{\rm sym}(n, T) = \frac{1}{2} \left. \frac{\partial^2 E_A}{\partial \delta^2} \right|_{\delta=0} . \quad (79)$$

Usually, the dependence of $E_A(n, \delta, T)$ for the complete range of asymmetries is quite well approximated by a quadratic function. In this case the symmetry energy also represents the difference between the binding energy per nucleon of neutron matter and of symmetric nuclear matter. At finite temperatures one must distinguish between the internal symmetry energy $E_{\rm sym}(n, T)$ and the free symmetry energy $F_{\rm sym}(n, T)$ that is similarly defined.

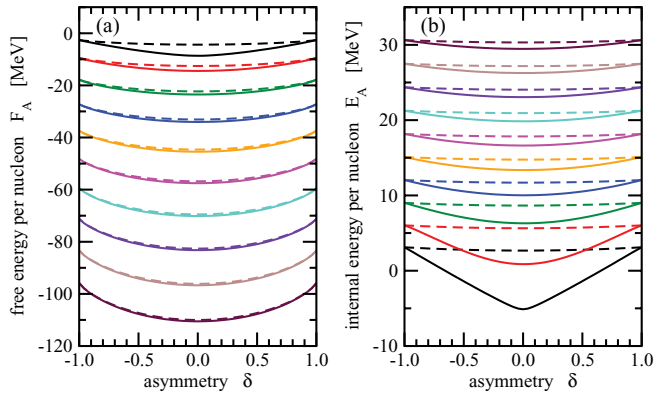

FIG. 12. (Color online) Free energy per nucleon F_A (left) and internal energy per nucleon E_A (right) as a function of the asymmetry δ for constant total density $n = 0.001\,\mathrm{fm}^{-3}$ for various temperatures T without light clusters (dashed lines) and with light clusters (solid lines). See Fig 2 for the color code.

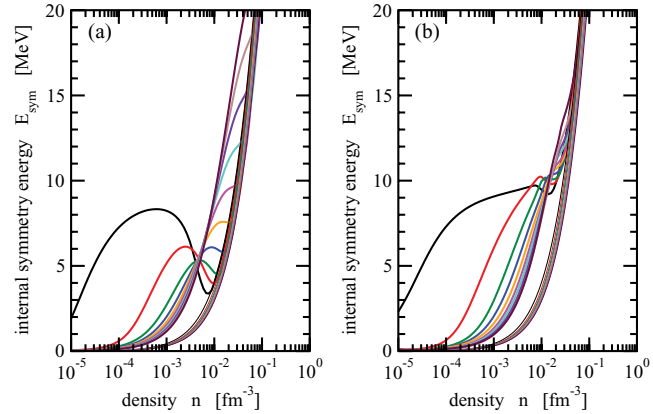

FIG. 13. (Color online) Internal symmetry energy E_{sym} as a function of the total density n for various temperatures T in the generalized RMF model (a) and the QS approach (b) with light clusters (thick solid lines). The results of the RMF calculation without clusters are denoted by thin solid lines for low densities. See Fig. 2 for the color code.

However, the quadratic approximation is not valid in general, especially for a system with cluster correlations at densities n below the nuclear saturation density. This is clearly seen for our models in the dependence of E_A and F_A on δ for given n and T. In Fig. 12 the free binding energy per nucleon (left) and the internal binding energy per nucleon (right) are shown as a function of the asymmetry for a fixed density $n = 0.001\,\mathrm{fm}^{-3}$ and different temperatures. Without clusters, the dependence on δ is rather weak and can be well described by a parabolic function irrespective of the temperature. With clusters, the binding energies per nucleon are substantially lowered around $\delta = 0$, that is, symmetric nuclear matter, particularly for low temperatures. The system gains additional binding energy by forming clusters. Large deviations from a global quadratic dependence develop and especially at low temperatures the parabola changes to a triangular shape, most obviously seen for the internal energy per nucleon. This behavior leads to a very large and thus not very meaningful symmetry energy in the limit $T \to 0\,\mathrm{MeV}$ when the conventional definition (79) is used. Hence, a more appropriate characterization for the symmetry energy is required. A reasonable choice is given by the finite difference formula

$$E_{\mathrm{sym}}(n,T) = \tfrac{1}{2}[E_A(n,1,T) - 2E_A(n,0,T) + E_A(n,-1,T)], \tag{80}$$

which is identical to Eq. (79) for an exact quadratic dependence of the internal binding energy per nucleon on δ. This modified definition gives a good measure of the binding energy differences between neutrons, protons, and symmetric nuclear matter. A corresponding equation defines the free symmetry energy $F_{\mathrm{sym}}(n,T)$.

The density dependence of the internal symmetry energy E_{sym} and of the free symmetry energy F_{sym} as defined previously is presented in Figs. 13 and 14, respectively, as a function of density for various temperatures. In these figures, the results of the RMF and QS approaches with clusters are compared to the RMF result without clusters. Just as for the free energy, Fig. 7, and the internal energy, Fig. 8, of symmetric nuclear matter, the free and internal symmetry energies exhibit a different behavior for $n \to 0$. In all models, E_{sym} approaches zero in this limit, but F_{sym} converges to $T \ln 2$.

In the RMF model without clusters both internal and free symmetry energies rise continuously with increasing density, and E_{sym} is almost independent of T. When the formation of clusters is taken into account, the internal symmetry energy increases substantially at low densities (see Fig. 13). This behavior is caused by the additional binding of symmetric nuclear matter, which was already seen in Fig. 12, that is particularly pronounced at low temperatures with a large cluster fraction. The density dependence of the internal symmetry energy is rather different for the for the RMF and QS approaches in a region near $10^{-2}\,\mathrm{fm}^{-3}$. As discussed in Sec. IV A, in the RMF calculation the fraction of deuterons is enhanced in the transition region whereas three- and four-body

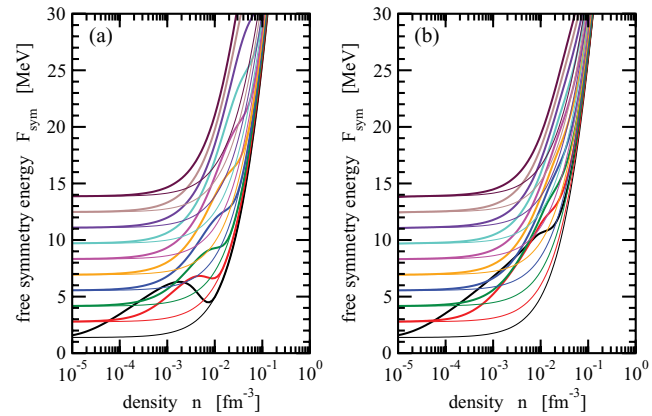

FIG. 14. (Color online) Free symmetry energy F_{sym} as a function of the total density n for various temperatures T in the generalized RMF model (a) and the QS approach (b) with light clusters (thick solid lines). The results of the RMF calculation without clusters are denoted by thin solid lines for low densities. See Fig. 2 for the color code.

correlations are suppressed as compared to the QS approach. Correspondingly, symmetric nuclear matter is less bound here and the symmetry energy is reduced relative to the QS approach. Because two-body correlations survive in the RMF model to too high densities for larger temperatures, the internal symmetry energy is also lowered considerably when the total baryon number density approaches the saturation density. In the QS approach, E_A is much closer to the RMF result without clusters with increasing density. The free symmetry energy, see Fig. 14, shows essentially the same features as the internal symmetry. However, they are less pronounced because of the different low-temperature limit.

VII. COMPARISON WITH OTHER APPROACHES

We discuss light cluster abundances obtained from our approaches in comparison with results from other models, which appear in the literature and which have been discussed in this article. These are the EoS of Shen *et al.* [29], an EoS based on a virial expansion as presented in Ref. [32], and a nuclear statistical equilibrium calculation that takes into account the ground states of all nuclei in the atomic mass evaluation (AME 2003) [60]. Figure 15 shows the α-particle fraction in symmetric nuclear matter at four different temperatures as a function of density. We have not explicitly included the results of the model of Lattimer and Swesty [28] in this comparison. They use the same excluded volume prescription as Shen *et al.* [29] to take into account the medium dependence of the α-particle fraction. Therefore, the behavior with density of

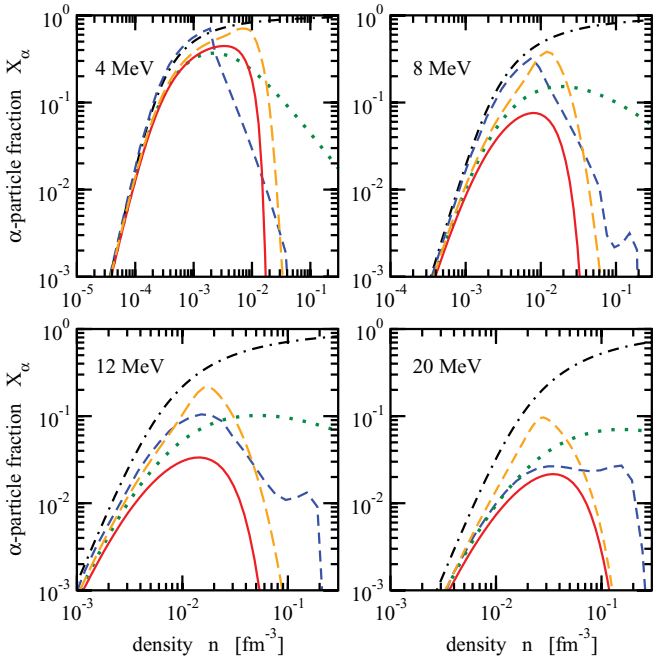

FIG. 15. (Color online) Comparison of α-particle fractions in symmetric nuclear matter as a function of the density at four temperatures for the virial expansion (black dashed-dotted lines), NSE (green dotted lines), the EoS of Shen *et al.* [29] (blue dashed lines), the generalized RMF model (red solid lines), and the QS approach (orange dashed lines). Note the different scales on the x axes.

their results is similar to that of Shen *et al.* [29], even though absolutely there are differences due to a different treatment of the heavy particle fraction. A direct comparison of X_α of Shen *et al.* [29] and Lattimer *et al.* [28] can be found in Ref. [31].

At low densities all models show a decreasing α-particle fraction with decreasing total baryon number density. However, there are some subtle differences. The virial expansion (black dash-dotted lines) takes scattering contributions to the second virial coefficient into account. These are important at higher temperatures and cause a slightly higher prediction for X_α at small n. The effect of cluster dissociation is absent in this model and results in a monotonic increase of the cluster fraction with increasing density, which is unphysical because one does not expect to see clusters in nuclear matter at saturation density.

The NSE approach (green dotted lines) compared to the virial approach shows a reduction of the α-particle fraction at all densities, due to the formation of heavier clusters. The α-particles survive even beyond the nuclear saturation density, because medium modification and dissolution of clusters are absent in this model, which also fails to describe the transition from clusterized matter to cluster-free nuclear matter at high densities.

The Shen *et al.* [29] EoS (blue dashed lines) neglects the contribution of deuteron, triton, and helion clusters. This leads to an overestimation of the α-particle fraction at low densities where actually lighter clusters dominate the composition. In contrast to the aforementioned two approaches, there is a steep decrease of the α-cluster abundance when approaching the saturation density. However, one notes some irregularities that are understood as an effect of the excluded volume approach when the closest packing is reached.

The generalized RMF model (red solid lines) developed in this work describes the decrease of the α-particle fraction at high densities by a reduction of their binding energy due to the Pauli blocking that leads to the Mott effect for vanishing binding. The maximum cluster density is reached around the Mott density. Because of the presence of strong correlations in the scattering state continuum that are effectively represented by one resonance, there is a nonvanishing cluster fraction above the Mott density. Among all models presented in the comparison of Fig. 15, the generalized RMF approach shows the strongest reduction of the α-cluster fraction.

In the QS approach the behavior of the density dependence of X_α is similar to that of the generalized RMF model, but has for all densities a higher α-cluster fraction, which is accompanied by smaller light cluster abundances. As discussed in Sec. IV A the difference in X_α between the two models is mainly due to the overemphasis of the deuteron correlations in the RMF model, which suppresses the α-particle fraction. On the other hand, the RMF model takes into account the back reaction of the cluster formation on the mean field that is missing in the QS approach.

The difference between the two approaches of this article, shown in Fig. 15, in direct comparison, also gives an indication of the effects of possible improvements in the models, apart, of course, from the inclusion of heavier clusters, i.e. nuclei embedded in a clusterized gas. However, the synopsis of Fig. 15 demonstrates the advantage of systematic

many-body approaches to the description of cluster formation over alternative approaches that lack a microphysical mechanism to account for the cluster breakup, but that are extensively used, for examle, in astrophysical applications.

VIII. CONCLUSIONS

Up to now there exist different strategies to model the EoS of nuclear matter and, in particular, to extract the symmetry energy: (1) phenomenological density functional methods, such as nonrelativistic Skyrme or relativistic RMF functionals, (2) effective-field theory approaches based on density functional or chiral perturbation theory, or (3) *ab initio* approaches, such as Brueckner-type methods, variational calculations, or Green function methods. A recent overview of these methods with references can be found, for example, in Ref. [51]. These methods are developed to obtain reliable equations of state for nuclear matter for a range of densities and asymmetries. In particular, the density-dependent RMF model can be considered phenomenologically a very useful approach in this respect because it has been applied with great success in the simultaneous description of cold nuclear matter in finite nuclei and compact stars as well as of hot nuclear matter in heavy-ion collisions and supernova explosions. However, all these approaches fail in the low-density limit, where cluster formation becomes essential. In this region, simple approaches that take clusters into account, such as the NSE or the Beth-Uhlenbeck formula of the virial expansion, show that clusters give a substantial contribution to the composition and the thermodynamic properties. However, models like the NSE or the virial expansion fail at higher densities where in-medium effects become important leading to a dissolution of clusters and the transition to cluster-free nuclear matter.

Here we propose, for the first time, a unified treatment that takes both limits into account describing the smooth transition from clusterized matter at low densities to pure nucleonic matter at high densities. We thus suggest a symbiotic framework that combines the merits of a QS approach in describing cluster properties in a medium with those of the RMF approach to model nucleonic self-energy effects, resulting in two hybrid approaches to the problem of cluster formation and dissolution. On the one hand we use a microscopic QS approach to describe the medium modification of cluster binding energies due to Pauli blocking. In this approach we employ nucleon self-energies taken in parametrized form from a very recent version of the density-dependent RMF model. On the other hand, the results of the QS approach for the cluster properties inside the medium are incorporated into an effective hadronic field theory using a Lagrangian formulation. Such a theory already has the correct high-density behavior as deduced from comparisons to heavy-ion collision experiments. We improve the low-density behavior by explicitly including light clusters, such as deuterons, tritons, helions, and α-particles, as explicit degrees of freedom taking into account the medium modification of their binding energies from the results of the QS approach.

In the numerical evaluation of both hybrid approaches developed in this work, we find that well-defined clusters appear only for densities below approximately $1/10$ to $1/100$ of the saturation density and get dissolved at higher densities. A direct confirmation of the given approach can be obtained from a comparison with recent results from heavy-ion collisions at low energies [8]. These investigations indicate larger values for the symmetry energy in comparison with the mean-field results at low densities, which seem to be in agreement with our findings [63].

Realistic approaches to the clustering in low-density nuclear matter should include excited states such as resonances and also the contribution of the continuum of scattering states. This can be done for the second virial coefficient, as demonstrated by the generalized Beth-Uhlenbeck approach [41]. In this way one can also reach the exact low-density limit of the virial approach [31–33]. Compared with the approaches of Lattimer and Swesty [28] and Shen *et al.* [29], who employ phenomenological concepts such as the excluded volume, we have given in this work a description of medium effects on the clusters and of their breakup as a result of the fundamental Pauli principle.

The extension of the present framework to larger clusters beyond the α particle is straightforward along the lines given in this work. For the evaluation of self-energies and Pauli shifts of A-particle clusters in nuclear matter, see Ref. [59]. The generalization of the given approach to account for clusters of arbitrary size would lead to an improvement in the low-density limit when comparing the nuclear statistical equilibrium as used, for example, in multifragmentation models [64,65]. One can alternatively also introduce the formation of heavier nuclei [59] in the presence of a nucleon and cluster gas, in a manner similar to the way it was done in the Thomas-Fermi approximation in the Shen *et al.* [29] approach. This will be relegated to a subsequent article. We restricted our present work to that region of the phase diagram where heavier clusters with $A > 4$ are not relevant.

In our models, we constructed the phase transition from clusterized, gaseous low-density matter to a cluster-free nuclear liquid at high densities. The coexistence region gives a hint about the range in temperature and density where the occurrence of inhomogeneities and the formation of heavy clusters become relevant. An issue for future investigations is an improved description near the phase transition taking into account effects of the Coulomb interaction and charge screening.

We are able to give the composition and the thermodynamic quantities in a large region of densities, temperatures, and asymmetries as they are required, for example, in supernova simulations. We did not consider contributions from, for example, electrons, neutrinos, or photons, to the thermodynamical quantities. In astrophysical applications of the EoS, they must be included. They will modify the properties of the system and affect, in particular, the occurrence of inhomogeneities and of the liquid-gas phase transition.

As a long-range objective, we aim at a unified description of nuclear matter from very low density to, eventually, the deconfinement phase transition that is based on a more microscopic and self-contained description than previous approaches to the EoS that have been used up to now in astrophysical models.

ACKNOWLEDGMENTS

This research was supported by the DFG cluster of excellence "Origin and Structure of the Universe" and by CompStar, a Research Networking Programme of the European Science Foundation. The work of TK was supported by the Department of Energy, Office of Nuclear Physics, Contract DE-AC02-06CH11357. DB acknowledges support from the Polish Ministry for Research and Higher Education under Grants N N202 0953 33 and N N202 2318 37 and from the Russian Fund for Fundamental Investigations under Grant 08-02-01003-a.

APPNDIX: LOW-DENSITY EXPANSION

A density-dependent RMF model was considered in Ref. [45]. The following low-density expansions are derived from this model and reproduce the DD-RMF results below the baryon density $n \leqslant 0.2\,\mathrm{fm}^{-3}$ within 0.1 %; variables are the total baryon density $n = n_p^{\mathrm{tot}} + n_n^{\mathrm{tot}}$ in units of fm^{-3}, the asymmetry $\delta = (n_p^{\mathrm{tot}} - n_n^{\mathrm{tot}})/(n_p^{\mathrm{tot}} + n_n^{\mathrm{tot}})$, and the temperature T in MeV. The scalar field in MeV is given by

$$\begin{aligned}\Sigma_{n,p}(T,n,\delta) = n_B[&(4524.13 - 6.926T) - 14.5157\,\delta^2/4 \\ &+ 0.833943\,\delta^4/16 - 9.00693\,\delta^6/64] \\ &+ n^2[-19190.7 - 2426.57\,\delta^2/4 - 317.732\,\delta^4/16 \\ &- 1547.38\,\delta^6/64] + n^3[62169.5 + 2521.29\,\delta^2/4 \\ &+ 3470.28\,\delta^4/16] + n^4[-91005.1 \\ &+ 3984.82\,\delta^2/4 - 9148.6\,\delta^4/16], \end{aligned} \tag{A1}$$

and the vector field in MeV by

$$\begin{aligned}\Sigma_p^0(T,n,\delta) = \Sigma_n^0(T,n,-\delta) = n[&3462.24 + 946.705\,\delta/2 \\ &- 0.334508\,\delta^2/4] + n^2[-11312.4 - 6246.21\,\delta/2 \\ &- 6353.53\,\delta^2/4 - 0.099478\,\delta^3/8] + n^3[20806.1 \\ &+ 18717.6\,\delta/2 + 29298\,\delta^2/4 - 0.490543\,\delta^3/8] \\ &+ n^4[352.371 - 24887.2\,\delta/2 - 39807.4\,\delta^2/4 \\ &- 0.346218\,\delta^3/8]. \end{aligned} \tag{A2}$$

The vector field is nearly independent of temperature, and the scalar field has a weak temperature dependence.

[1] P. Danielewicz, R. Lacey, and W. G. Lynch, Science **298**, 1592 (2002).
[2] C. Fuchs, A. Faessler, E. Zabrodin, and Y. M. Zheng, Phys. Rev. Lett. **86**, 1974 (2001).
[3] G. Ferini, T. Gaitanos, M. Colonna, M. Di Toro, and H. H. Wolter, Phys. Rev. Lett. **97**, 202301 (2006).
[4] V. Baran, M. Colonna, V. Greco, and M. Di Toro, Phys. Rep. **410**, 335 (2005).
[5] A. W. Steiner, M. Prakash, J. M. Lattimer, and P. J. Ellis, Phys. Rep. **411**, 325 (2005).
[6] B. A. Li, L. W. Chen, and C. M. Ko, Phys. Rep. **464**, 113 (2008).
[7] A. Tohsaki, H. Horiuchi, P. Schuck, and G. Röpke, Phys. Rev. Lett. **87**, 192501 (2001).
[8] S. Kowalski *et al.*, Phys. Rev. C **75**, 014601 (2007).
[9] B. A. Brown, Phys. Rev. Lett. **85**, 5296 (2000).
[10] S. Typel and B. A. Brown, Phys. Rev. C **64**, 027302 (2001).
[11] L. W. Chen, C. M. Ko, and B. A. Li, Phys. Rev. Lett. **94**, 032701 (2005); Phys. Rev. C **72**, 064309 (2005); **76**, 054316 (2007).
[12] R. J. Furnstahl, Nucl. Phys. **A706**, 85 (2002).
[13] M. Baldo, C. Maieron, P. Schuck, and X. Viñas, Nucl. Phys. **A736**, 241 (2004).
[14] S. S. Avancini, J. R. Marinelli, D. P. Menezes, M. M. W. Moraes, and C. Providência, Phys. Rev. C **75**, 055805 (2007).
[15] M. Centelles, X. Roca-Maza, X. Viñas, and M. Warda, Phys. Rev. Lett. **102**, 122502 (2009).
[16] M. Warda, X. Viñas, X. Roca-Maza, and M. Centelles, Phys. Rev. C **80**, 024316 (2009).
[17] C. J. Horowitz, S. J. Pollock, P. A. Souder, and R. Michaels, Phys. Rev. C **63**, 025501 (2001); http://hallaweb.jlab.org/parity/prex.
[18] T. Klähn *et al.*, Phys. Rev. C **74**, 035802 (2006).
[19] S. S. Avancini, L. Brito, J. R. Marinelli, D. P. Menezes, M. M. W. de Moraes, C. Providencia, and A. M. Santos, Phys. Rev. C **79**, 035804 (2009).
[20] C. J. Horowitz, and D. K. Berry, Phys. Rev. C **78**, 035806 (2008).
[21] H. Sonoda, G. Watanabe, K. Sato, T. Takiwaki, K. Yasuoka, and T. Ebisuzaki, Phys. Rev. C **75**, 042801(R) (2007).
[22] T. Maruyama, T. Tatsumi, T. Endo, and S. Chiba, Recent Res. Devel. Physics. **7**, 1 (2006).
[23] W. G. Newton, J. R. Stone, and A. Mezzacappa, J. Phys. Conf. Ser. **46**, 408 (2006).
[24] J. M. Lattimer and M. Prakash, Science **304**, 536 (2004).
[25] H. Dimmelmeier, C. D. Ott, H. T. Janka, A. Marek, and E. Muller, Phys. Rev. Lett. **98**, 251101 (2007).
[26] H. Dimmelmeier, C. D. Ott, A. Marek, and H. T. Janka, Phys. Rev. D **78**, 064056 (2008).
[27] K. Sumiyoshi and G. Röpke, Phys. Rev. C **77**, 055804 (2008).
[28] J. M. Lattimer and F. D. Swesty, Nucl. Phys. **A535**, 331 (1991).
[29] H. Shen, H. Toki, K. Oyamatsu, and K. Sumiyoshi, Prog. Theor. Phys. **100**, 1013 (1998); Nucl. Phys. **A637**, 435 (1998).
[30] B. D. Serot and J. D. Walecka, Adv. Nucl. Phys. **16**, 1 (1986).
[31] C. J. Horowitz and A. Schwenk, Phys. Lett. **B642**, 326 (2006).
[32] C. J. Horowitz and A. Schwenk, Nucl. Phys. **A776**, 55 (2006).
[33] E. O'Connor, D. Gazit, C. J. Horowitz, A. Schwenk, and N. Barnea, Phys. Rev. C **75**, 055803 (2007).
[34] S. Mallik, J. N. De, S. K. Samaddar, and S. Sarkar, Phys. Rev. C **77**, 032201(R) (2008).
[35] S. Heckel, P. P. Schneider, and A. Sedrakian, Phys. Rev. C **80**, 015805 (2009).
[36] G. E. Uhlenbeck and E. Beth, Physica **3**, 729 (1936); E. Beth and G. E. Uhlenbeck, *ibid.* **4**, 915 (1937).
[37] G. Röpke, H. Schulz, and L. Münchow, Nucl. Phys. **A379**, 536 (1982).
[38] G. Röpke, M. Schmidt, L. Münchow, and H. Schulz, Nucl. Phys. **A399**, 587 (1983).
[39] G. Röpke, T. Seifert, H. Stolz, and R. Zimmermann, Phys. Status Solidi B **100**, 215 (1980).
[40] J. Dukelsky, G. Röpke, and P. Schuck, Nucl. Phys. **A628**, 17 (1998).
[41] M. Schmidt, G. Röpke, and H. Schulz, Ann. Phys. (NY) **202**, 57 (1990).

[42] G. Röpke, M. Schmidt, L. Münchow, and H. Schulz, Phys. Lett. **B110**, 21 (1982).
[43] M. Beyer, W. Schadow, C. Kuhrts, and G. Röpke, Phys. Rev. C **60**, 034004 (1999); M. Beyer, S. A. Sofianos, C. Kuhrts, G. Röpke, and P. Schuck, Phys. Lett. **B488**, 247 (2000).
[44] A. Sedrakian and J. W. Clark, Phys. Rev. C **73**, 035803 (2006).
[45] S. Typel, Phys. Rev. C **71**, 064301 (2005).
[46] D. Vautherin and D. M. Brink, Phys. Rev. C **5**, 626 (1972).
[47] J. Margueron, E. van Dalen, and C. Fuchs, Phys. Rev. C **76**, 034309 (2007).
[48] J. Haidenbauer and W. Plessas, Phys. Rev. C **30**, 1822 (1984); L. Mathelitsch, W. Plessas, and W. Schweiger, *ibid.* **26**, 65 (1982).
[49] R. B. Wiringa, V. G. J. Stoks, and R. Schiavilla, Phys. Rev. C **51**, 38 (1995).
[50] S. C. Pieper and R. B. Wiringa, Annu. Rev. Nucl. Part. Sci. **51**, 53 (2001).
[51] C. Fuchs and H. H. Wolter, Eur. Phys. J. A **30**, 5 (2006).
[52] T. Alm, G. Röpke, A. Schnell, N. H. Kwong, and H. S. Köhler, Phys. Rev. C **53**, 2181 (1996); H. J. Schulze, A. Schnell, G. Röpke, and U. Lombardo, *ibid.* **55**, 3006 (1997).
[53] E. N. E. van Dalen, C. Fuchs, and A. Faessler, Phys. Rev. Lett. **95**, 022302 (2005).
[54] G. Röpke, A. Grigo, K. Sumiyoshi, and Hong Shen, Pisma Fiz. Elem. Chast. Atom. Yadra **2**, 25 (2005) [Phys. Part. Nucl. Lett. **2**, 275 (2005)].
[55] G. Röpke, A. Grigo, K. Sumiyoshi, and Hong Shen, in *Superdense QCD Matter and Compact Stars*, NATO Science Series II: Mathematics, Physics and Chemistry, Vol. 197, edited by D. Blaschke and D. Sedrakian (Springer, Dordrecht, 2006), p. 75.
[56] G. Röpke, Phys. Rev. C **79**, 014002 (2009).
[57] S. Shlomo and V. M. Kolomietz, Rep. Prog. Phys. **68**, 1 (2005).
[58] A. Kolomiets, V. M. Kolomietz, and S. Shlomo, Phys. Rev. C **55**, 1376 (1997).
[59] G. Röpke, M. Schmidt, and H. Schulz, Nucl. Phys. **A424**, 594 (1984).
[60] G. Audi, A. H. Wapstra, and C. Thibault, Nucl. Phys. **A729**, 337 (2002).
[61] M. Barranco and J. R. Buchler, Phys. Rev. C **22**, 1729 (1980).
[62] H. Müller and B. D. Serot, Phys. Rev. C **52**, 2072 (1995).
[63] J. B. Natowicz, arXiv:1001.1102 [nucl-th].
[64] J. P. Bondorf, A. S. Botvina, A. S. Ilinov, I. N. Mishustin, and K. Sneppen, Phys. Rep. **257**, 133 (1995).
[65] D. H. E. Gross, Rep. Prog. Phys. **53**, 605 (1990).